

Hydrogen “penta-graphene-like” structure stabilized by hafnium: a high-temperature conventional superconductor

Hui Xie¹, Yansun Yao², Xiaolei Feng^{3,4}, Defang Duan^{1,5,*}, Hao Song¹, Zihan Zhang¹, Shuqing Jiang¹,
Simon A. T. Redfern⁶, Vladimir Z. Kresin⁷, Chris J. Pickard^{5,8,*} and Tian Cui^{9,1,*}

¹*State Key Laboratory of Superhard Materials, college of Physics, Jilin University, Changchun 130012, China*

²*Department of Physics and Engineering Physics, University of Saskatchewan, Saskatoon, Saskatchewan S7N 5E2, Canada*

³*Center for High Pressure Science and Technology Advanced Research, Beijing 100094, China*

⁴*Department of Earth Science, University of Cambridge, Downing Site, Cambridge CB2 3EQ, United Kingdom*

⁵*Department of Materials Science & Metallurgy, University of Cambridge, 27 Charles Babbage Road, Cambridge CB3 0FS, United Kingdom*

⁶*Asian School of the Environment, Nanyang Technological University, Singapore 639798*

⁷*Lawrence Berkeley Laboratory, University of California at Berkeley, Berkeley, CA 94720, USA*

⁸*Advanced Institute for Materials Research, Tohoku University 2-1-1 Katahira, Aoba, Sendai, 980-8577, Japan*

⁹*School of Physical Science and Technology, Ningbo University, Ningbo, 315211, People's Republic of China*

*Corresponding authors email: duandf@jlu.edu.cn, cjp20@cam.ac.uk, cuitian@jlu.edu.cn

Abstract

The recent discovery of H_3S and LaH_{10} superconductors with record high superconducting transition temperatures, T_c , at high pressure, has fueled the search for room-temperature superconductivity in the compressed superhydrides. Here we predict the existence of an unprecedented hexagonal HfH_{10} , with an extraordinarily high T_c of around 213-234 K at 250 GPa. In HfH_{10} , the H atoms are arranged in clusters to form a planar “penta-graphene-like” sublattice, in contrast to the covalent sixfold cubic structure in H_3S and clathrate-like structure in LaH_{10} . The Hf atom acts as a “precompressor” and electron donor to the hydrogen sublattice. This “penta-graphene-like” H_{10} structure is also found in ZrH_{10} , ScH_{10} and LuH_{10} at high pressure, each material showing a high T_c ranging from 134 to 220 kelvin. Our study of dense superhydrides with “penta-graphene-like” layered structures opens the door to the exploration and exploitation of a new class of high T_c superconductors.

Main

The development of room temperature superconductors is the ultimate goal for superconductivity research. The Bardeen-Cooper-Schrieffer (BCS) theory suggests that metallic hydrogen is likely to be a good candidate for attaining high-temperature superconductivity, due to its high Debye temperature and strong electron-phonon coupling¹⁻². Conceptually, metallization can be achieved in pure hydrogen by dissociating the H₂ molecules under extreme conditions. Evidence for molecular dissociation has been found in high-pressure phases of solid hydrogen, where the vibron frequency decreases rapidly with increasing pressure³, indicating the weakening of the intramolecular bonding along the way to transition to the metallic state. However, although there have been extensive attempts to synthesize metallic hydrogen⁴⁻⁵, there is a lack of consensus on reported “successes”, and superconductivity has not been measured in any of the reported phases.

In the face of tremendous difficulties in the synthesis of pure metallic hydrogen, many investigators have suggested that metallization can be achieved through an alternative approach, by ‘precompressing’ hydrogen species in a matrix of another element⁶, forming a compound. Specifically, highly compressed hydrogen-dominant hydrides are predicted to be able to attain a metallic state and may, therefore, exhibit high T_c superconductivity due to such ‘chemical precompression’ since the charge density required for metallization can be achieved at lower pressure than that required for pure hydrogen. Recently, the search for high- T_c superconductivity has been expanded from the known species⁷⁻⁹ to hitherto unknown hydrides, through high-pressure synthesis following theoretical predictions¹⁰⁻²³. Remarkably, two of the predicted hydrides, H₃S¹¹⁻¹³ and LaH₁₀¹⁷⁻¹⁹, have been successfully synthesized recently and exhibit record high T_c above 200 K. H₃S has a *bcc* lattice of S with H atoms located halfway between the S atoms, exhibiting three-dimensional covalent metallic characteristics. LaH₁₀ has a three-dimensional clathrate-like structure of H with La atoms filling the clathrate cavities, and has been described as an extended metallic hydrogen host structure stabilized by the guest electron donor (La).

By analyzing the superconducting properties of a large number of hydrides, we have summarized four criteria for finding high temperature superconductors in highly compressed hydrides: (i) high symmetry crystal structure, (ii) absence of H₂-like molecular units, (iii) a large H contribution to the

total electronic density of states (DOS) at the Fermi level, and (iv) strong coupling of electrons on the Fermi surface with high frequency phonons. The search for high- T_c materials has been focused on two families of binary hydrides [see Table S1], covalent sixfold cubic structure¹⁰⁻¹⁴ found in H_3S and H_3Se , and clathrate structure¹⁵⁻²² found in rare earth hydrides REH_{10} , REH_9 and REH_6 . These two high- T_c families satisfy the mentioned four criteria, with a common feature that they both adopt three-dimensional sublattices of hydrogen. On the other hand, pure solid hydrogen features pronounced layer-like characters. A prominent example is the phase IV of hydrogen that consists of strongly bonded H_2 molecules and weakly bonded graphene-like sheets²⁴⁻²⁶. This structure is considered an important intermediate between the molecular (insulating) and atomic (metallic) crystalline phases of hydrogen. Many hydrides have been predicted to have a layered structure, but their T_c are not very high, *e.g.* FeH_5 ²⁷, TeH_4 ²⁸, and KH_6 ²⁹, etc. One can raise the following question: is there a two-dimensional structure of hydrogen-rich materials at high pressure that can achieve high T_c ?

To answer this question, we performed an extensive material searching at high-pressure and discovered that a layered hexagonal hafnium decahydride (HfH_{10}) indeed has an extraordinarily high T_c . In HfH_{10} , the H atoms form planar clusters of three H_5 pentagons, analogous to penta-graphene, while Hf atoms are intercalated between the clusters on the same plane. A new class of superhydrides, MH_{10} ($M = Zr, Sc$ and Lu), which are isostructural with HfH_{10} , have also been predicted to be stable or metastable at high pressure, and all are predicted to possess high superconducting T_c .

Structures of new hydrides and their stabilities

Our main structure searching results for Hf-H system at high pressure are depicted in the convex hull diagrams of Fig. 1 and S1. Considering the non-negligible quantum effects associated with hydrogen, the zero-point energy (ZPE) was calculated and included in the calculation of the formation enthalpies of predicted Hf-H compounds. We analyzed the stability of these compounds with respect to the elemental hafnium and hydrogen end members. As shown in Fig. 1(a), these searches revealed five stable stoichiometries at various pressures, *e.g.*, HfH , HfH_3 , HfH_4 , HfH_6 and HfH_{10} , in addition to the previously known HfH_2 and Hf_4H_{15} ³⁰⁻³¹. The crystal structures of the predicted compounds are illustrated in Figs. 1(b) and S2. In HfH_x ($x = 1$ to 4), all hydrogen atoms are present in atomic form. In HfH_6 , only three hydrogen atoms are in atomic form while the other three form an H_3 unit. For HfH_{10} ,

there are two energetically competitive structures, one adopting a $P6_3/mmc$ structure and the other in $P\bar{1}$ symmetry. At 300 GPa, The $P\bar{1}$ structure is calculated to be more enthalpically favorable than the $P6_3/mmc$ structure, but the latter is slightly more stable once the ZPE is included, with the energy difference within 2 meV/atom. It is therefore argued here that the two structures are both valid structures for HfH₁₀. The $P\bar{1}$ structure consists of diatomic hydrogen pairs similar to H₂ molecules, and this violates criteria (i) and (ii) for attaining high T_c . Intriguingly, the $P6_3/mmc$ is a layered structure in which the Hf and H atoms are situated on the same plane [Fig. 1(b) and (c)]. The Hf atoms form a hexagonal sublattice interspersed by H atoms in unique ‘H₅’ pentagons akin to the geometry of pentagraphene: three pentagons are fused by edge-sharing to form a H₁₀ unit, as depicted in Fig. 1(c). In the proceeding discussion, the superhydride $P6_3/mmc$ -HfH₁₀ is the main focus because it satisfies both criteria (i) high crystal symmetry and (ii) absence of H₂ molecular unit.

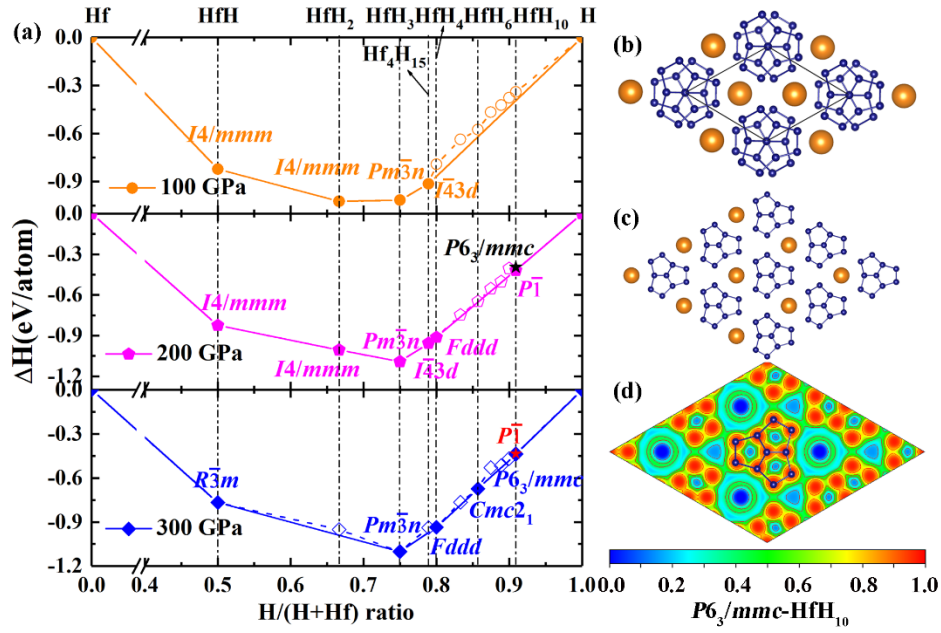


Fig. 1 | Convex hull of H-rich hafnium hydrides and structure motif of $P6_3/mmc$ -HfH₁₀. (a) Formation enthalpies of predicted HfH_x ($x=1-10$) selected from structure searches up to HfH₂₄ [see supplementary material], including ZPEs with respect to decomposition into Hf and H under pressure. The $Im\bar{3}m$ structure for hafnium³², the $P6_3/mc$, $C2/c$ and $Cmca$ -12 structures for hydrogen²⁵ were adopted. Open symbols represent unstable configurations with respect to mixing lines on the convex hull, while solid symbols on the convex hull represent stable configurations. The asterisk near convex hull represents the metastable structure. (b) The crystal structure of $P6_3/mmc$ structure in HfH₁₀, (c) a

single (001) plane, (d) ELF on the (001) plane. Golden (large) and small (blue) spheres represent Hf and H atoms, respectively.

We examine the chemical bonding of layered HfH₁₀ by analysing electron localization function (ELF), crystal orbital Hamiltonian population (COHP) and Bader charges. As shown in Figs. 1(d) and S3, there is no charge localization between Hf and H, indicating the Hf-H bonding is purely ionic. The ELF values for the H₁₀ unit range between 0.6-0.8, showing the evidence for H-H covalent bonding. As depicted in Fig. S4, the calculated COHP show that most of the states below the Fermi level correspond to H-H bonding for HfH₁₀, supporting the existence of H-H covalent bonds within the H₁₀ unit. Furthermore, Bader charge analysis reveals that the planar H₁₀ unit accepts an amount of charge, *e. g.*, $\sim 0.13 e^-$ per H atom, from nearby Hf atoms, which results in longer H-H distances compared to that in free H₂ molecule³³. The additional electrons reside in the H-H antibonding orbital (σ^*) and therefore weaken the H-H bonding, thus increasing the H-projected density of states (H-PDOS) at the Fermi level (ϵ_f).

To further explore this new form of hydrogen, we compared the H-H distances in HfH₁₀ with those in LaH₁₀¹⁷, atomic H₂ and layered phase-IV of H (*Pc*-48)²⁴ structures. As shown in Fig. S5, the longest nearest-neighbor H-H distance (d_{H1-H2}) in HfH₁₀ is close to the shortest H-H distance in LaH₁₀ at the same pressure. The distance between H1 and H2 (second nearest neighbor) atoms approaches that of the atomic structure of hydrogen near 200 GPa. As the pressure increases, the shortest H-H bond length (d_{H2-H3}) gets progressively closer to the H-H distances of *Pc*-48 H (d_2). Therefore, this “penta-graphene-like” hydrogen sublattice lies somewhere between atomic and layered hydrogen.

The discovery of apparently stable or metastable structures of HfH₁₀ prompt us to further study the Zr-H system at 300 GPa [see Fig. S6]. As might be anticipated, ZrH₁₀ adopts the same two competitive structures $P\bar{1}$ and $P6_3/mmc$ as HfH₁₀. For high-pressure synthesis, which usually also involves high temperatures, the experimentally realized materials often represent the metastable phases³⁴. The recently discovered high- T_c superconducting LaH₁₀¹⁸⁻¹⁹, for example, is a metastable compound lying above the convex hull that was previously predicted by Peng et al.¹⁶.

Evaluation of spectra and T_c for “penta-graphene-like” structure and pressure intervals

According to the criterion (iii) for high T_c superconductivity, a large H contribution to the total electronic DOS at the Fermi level is a critical factor for the development of exceptional superconducting properties. To this end, the projected electronic DOS of $P6_3/mmc$ in HfH₁₀ and ZrH₁₀ were calculated and are illustrated in Fig. 2. One can see that both phases are metallic with a large total electronic DOS and significant hydrogen contribution to the electronic DOS at the Fermi level. Remarkably, the electronic DOS exhibits van Hove singularities near the Fermi level, indicating a large electron-phonon coupling (EPC) strength bound up with hydrogen phonon modes. The total DOS of H₃S, LaH₁₀, HfH₁₀ and ZrH₁₀ at 300 GPa are compared in Fig. 2(c). It is shown that HfH₁₀ and LaH₁₀ have a comparable electronic DOS at the Fermi level, and these are notably larger than those of ZrH₁₀ and H₃S.

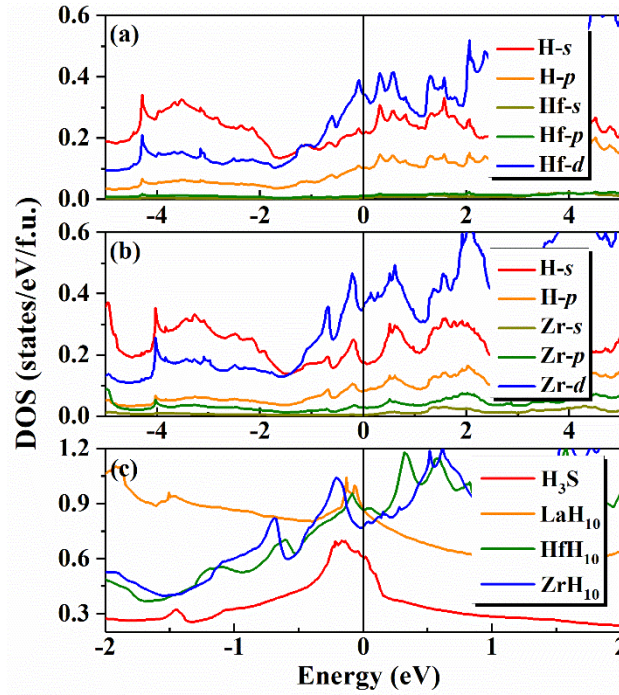


Fig. 2 | Calculated electronic DOS at 300 GPa. The projected electronic DOS of (a) $P6_3/mmc$ -HfH₁₀ and (b) $P6_3/mmc$ -ZrH₁₀. (c) The total electronic DOS of H₃S, LaH₁₀, HfH₁₀ and ZrH₁₀ around the van Hove singularities.

To examine the superconductivity in the “penta-graphene-like” structure, we calculate the average phonon frequency and EPC as shown in Table S4. For HfH₁₀, our EPC calculation yields a large λ of

2.16 at 300 GPa which is benefited from large H-PDOS and high frequency vibrations (above 10 THz) due to hydrogen which contribute 70 % to the value of λ [Fig. 3(a)]. It is obvious that the large λ satisfy the last criterion (iv). Since λ is larger than 1.5, we calculated T_c using three approaches: Allen-Dynes modified McMillian equation (A-D) [Eq. S12]³⁵, Matsubara-type linearized Eliashberg equation (LE)²¹, and Gor'kov-Kresin equation (G-K)³⁶, all of which were designed to estimate the T_c for materials with strong electron-phonon coupling. The results show that HfH₁₀ is an extraordinary superconductor with a T_c of 151-166 K (A-D), 214-228 K (LE), and 197-220 K (G-K) using $\mu^* = 0.1$ -0.13 at 300 GPa. To narrow down the range of T_c , we calculated the T_c of H₃S and LaH₁₀ at 200 GPa and compared them to the experimental values to obtain appropriate parameters for this family of materials. As presented in Fig. S7, the calculated T_c with $\mu^* = 0.13$ using G-K and LE equations are close to the experimental values, while those estimated by A-D equation are much lower. In the following, we will estimate the T_c 's using the G-K equation. With the pressure decreased to 250 GPa, λ and T_c for HfH₁₀ increase to 2.77 and 213-234 K with $\mu^* = 0.1$ -0.13, respectively; these values are higher than those for H₃S. For ZrH₁₀, a large EPC parameter λ of 1.59 is calculated at 300 GPa, of which 74% is due to contributions by H atoms [Fig. 3(b)]. A high superconducting transition temperature T_c of 194-218 K is therefore estimated for ZrH₁₀. At 250 GPa, T_c increases to 199-220 K with stronger λ of 1.77. We also calculated the electronic DOS and T_c of $P\bar{1}$ -HfH₁₀ at 200 GPa [see Fig. S8 and Table S6]. It is found that, as expected, the existence of H₂ units reduce the electronic DOS at the Fermi energy, and a low EPC parameter of 0.72, thereby limiting its superconductivity with T_c of 28.9-37.4 K ($\mu^* = 0.1$ -0.13). Therefore, the four criteria for superconductivity provide important guidance in the search for high-temperature superconductors in compressed superhydrides.

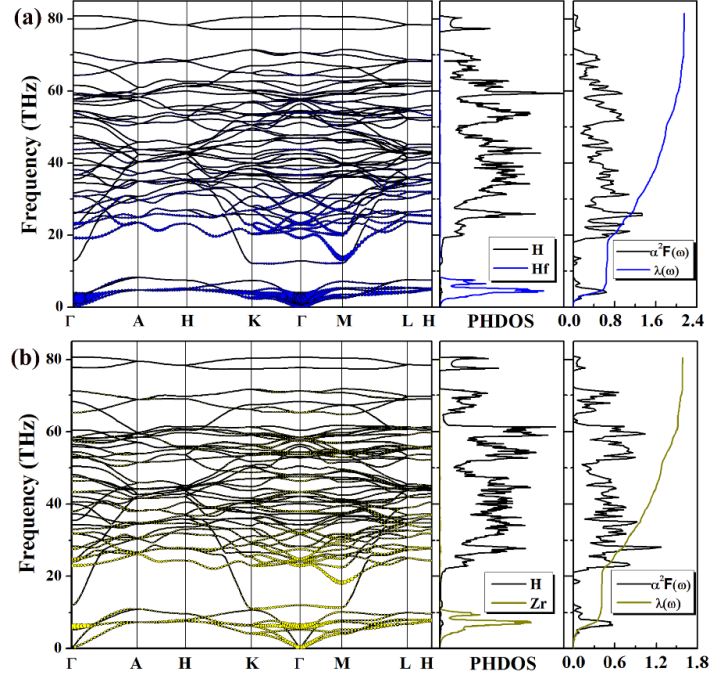


Fig. 3 | Phonon properties and Eliashberg spectral function for HfH₁₀ and ZrH₁₀ with *P6₃/mmc* structure. Phonon dispersion curves (left), density of states (middle) and Eliashberg spectral function $\alpha^2F(\omega)$ together with the electron-phonon integral $\lambda(\omega)$ (right) of (a) HfH₁₀ and (b) ZrH₁₀ at 300 GPa. The size of the solid dot on phonon spectra signifies the contribution to electron-phonon coupling.

To further understand the superconductivity of the ‘clathrate-like’ and “penta-graphene like” decahydrides, we compared the calculated T_c ’s and essential parameters for YH₁₀, LaH₁₀, HfH₁₀ and ZrH₁₀ at 300 GPa, illustrated in Fig. 4. We find that T_c decreases in the order of YH₁₀ > LaH₁₀ > HfH₁₀ > ZrH₁₀, consistent with the decreasing trend of optical superconducting transition temperature caused by the interaction of electrons with optical phonons (T_c^0), the contribution of H-PDOS to the total DOS at the Fermi level (P_H) and optical electron-phonon coupling (λ_{opt}). Thus, the high T_c in these hydrides is mainly attributed to the interaction of electrons with optical phonons and high DOS at the Fermi level associated with H atoms, in agreement with both superconducting criteria (iii) and (iv).

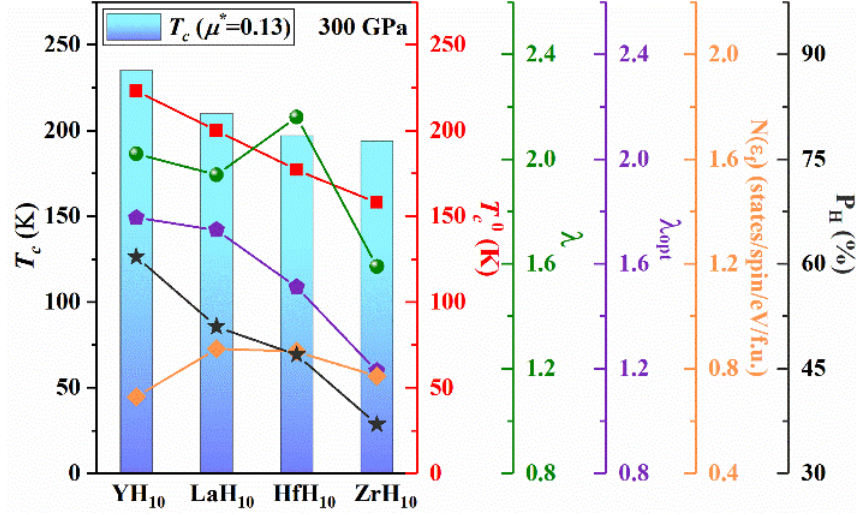


Fig. 4 | Calculated superconducting parameters for YH₁₀, LaH₁₀, HfH₁₀ and ZrH₁₀ at 300 GPa.

The superconducting critical temperature using G-K equation with $\mu^* = 0.13$ (T_c), the critical temperature caused by the interaction of electrons with optical phonons (T_c^0), EPC parameter (λ), strength of the interaction of electrons with optical phonons (λ_{opt}), electronic DOS at the Fermi level $N(E_f)$ and the contribution of H atoms DOS to the total DOS at the Fermi energy (P_H).

The fact that “penta-graphene like” HfH₁₀ and ZrH₁₀ have very high T_c naturally raises the question: can any other hydrides adopt the same structure and display high T_c as well? The elements of Hf and Zr have three features in common: similar Pauling electronegativity (~ 1.3), similar atomic radius (~ 1.6 Å), and d states in valence subshells. After searching the periodic table of elements, we found that Mg, Sc, Lu and Th have some similar properties. Phonon dispersion relations were calculated to test the stability of the corresponding decahydrides. The calculations did confirm that both ScH₁₀ and LuH₁₀ are dynamically stable, while MgH₁₀ and ThH₁₀ are not. For MgH₁₀ [Fig. S9] its dynamic instability could be due to the absence of d electrons in Mg and insufficient number of electrons transferred to H. For ThH₁₀ [Fig. S9], the large atomic radius of Th (1.8 Å) may be responsible for its dynamic instability. We note that the hexagonal structure $P6_3/mmc$ was first noted by Peng et al.¹⁶ for ScH₁₀. It was not discussed in depth, the main focus of this work being on the remarkable clathrate structure. Later, an orthogonal structure $Cmcm$ in ScH₁₀ was predicted³⁷. We thus calculate the enthalpies of $Cmcm$ and $P6_3/mmc$ phases as a function of pressure and find that these phases are indeed competitive [Fig. S10]. The electron-phonon coupling calculation for the $P6_3/mmc$ -

ScH₁₀ yields a λ of 1.16 and T_c ranging 134-158 K with $\mu^* = 0.1-0.13$ at 250 GPa [Figs. S11-S12]. For Lu-H system, we perform extensive structure searching and find that LuH₁₀ with $P6_3/mmc$ phase is stable at 300 GPa [Fig. S13]. Phonon calculation shows that it is dynamical stable down to at least 200 GPa [Fig. S14]. At 200 GPa, LuH₁₀ is found to be a good superconductor with a relatively high T_c of 134-152 K, comparable with to most other lanthanide hydrides. Although the emergence of $5d$ electron in Lu suppresses the contribution of $4f$ electrons and improves the contribution of hydrogen atoms at the Fermi level [Fig. S15], the relatively low total DOS at the Fermi level limits to some extent its superconductivity.

Isotope effect

Since the substitution of deuterium for hydrogen (H \rightarrow D) affects the optical modes only, whereas the value of T_c is affected by both acoustic and optical modes, the value of the isotope coefficient and its closeness to the $\alpha_{max} = 0.5$ reflects the relative impact of the high frequency optical modes on T_c and the interplay of the optical and acoustic modes. It is worth mentioning that the value of T_c would be reduced upon H \rightarrow D substitution, since the high frequency hydrogen modes determine the value of the critical temperature in high- T_c hydrides. Thus, the isotope coefficient (α) was calculated to estimate the T_c of MD₁₀ (T_c^D). As shown in Table S5, the coefficients are 0.42-0.43 for HfH₁₀ at 250 GPa, 0.38-0.39 for ZrH₁₀ at 250 GPa, 0.37-0.38 for ScH₁₀ at 250 GPa, and 0.44-0.45 for LuH₁₀ at 200 GPa with $\mu^* = 0.1-0.13$, respectively. The α values in these phases are relatively large, suggesting that the pairing, particularly in HfH₁₀ and LuH₁₀, is dominated by the optical H modes, which yields the relatively low T_c^D . The T_c^D was described according to the equation of $T_c/T_c^D = (M_H/M_D)^{-\alpha}$, where T_c is obtained from the G-K equation. In our cases, T_c^D values are 159-174 K for HfD₁₀, 153-168 K for ZrD₁₀, 104-121 K for ScD₁₀, and 99-111 K for LuD₁₀, respectively, providing a reference for future experiments.

New materials

Our extensive first-principles structure searches have revealed the appearance of stable or metastable “penta-graphene like” clustered H₁₀ structure in HfH₁₀, ZrH₁₀, ScH₁₀ and LuH₁₀. Electronegativity, atomic radius, and valence configuration of the metal element are all found to play

critical roles in the stabilization of this “penta-graphene like” hydrogen sublattice, and fine-tune the superconductivity of these materials. We want to pay a special attention to HfH_{10} which is predicted to be a high temperature superconductor with estimated T_c of 213-234 K at 250 GPa. It is the first example of two-dimensional structure in hydrogen-rich materials exhibiting high T_c above 200 K, which will encourage scientists to search for high-temperature superconductors in layered hydrogen-rich materials. It is also the hydride that has the highest T_c to date in the transition metal hydrides. This “penta-graphene like” clustered H_{10} structure is a structural model for superconducting hydrides with T_c higher than 200 K which is different from the covalent bonded H structure in H_3S and clathrate H structure in LaH_{10} . One can state that at present there are three different model structures for high T_c hydrides. The new structure model described in this paper further confirmed four criteria for high T_c superconductivity in hydrogen-rich material proposed in the beginning of the paper: (i) high symmetry is manifested by hexagonal structure $P6_3/mmc$, (ii) absence of H_2 -like molecular units; indeed, three H_5 pentagons fused a planar H_{10} clusters with the H-H distances which are between the values for the metallic phase and phase IV of solid hydrogen, (iii) a large H contribution to the total electronic density of states (DOS) at the Fermi level, which in this case is nearly one half, and (iv) strong coupling of electrons on the Fermi surface with high frequency phonons with large value of the coupling constant equal to 2.77. The emergence of “penta-graphene like” clustered H_{10} structure is quite significant, which will stimulate further study of the hydrogen-based family of new superconducting materials and certainly help to develop this promising field. The formulated four criteria for high T_c superconductivity provide a rationale for searching room-temperature superconductors in ternary or quaternary hydrogen-rich materials in the future, which have not been well explored to date.

Methods

We carried out extensive structure searches using Ab Initio Random Structure Searching (AIRSS), Crystal structure AnaLYsis by Particle Swarm Optimization (CALYPSO) and Universal Structure Predictor: Evolutionary Xtallography (USPEX)³⁸⁻⁴⁰ at pressures from 100 to 300 GPa, during which at least 15,000 structures were generated. Geometrical optimization calculations for Hf-H and Zr-H systems were performed using the on-the-fly generation of ultrasoft pseudopotentials with a plane-wave basis set energy cutoff of 800 eV, as implemented in CASTEP (Cambridge Sequential Total

Energy Package) code⁴¹. In ScH₁₀ and Lu-H cases, the all-electron projector-augmented wave method (PAW)⁴² pseudopotentials with a cutoff energy of 1000 eV were employed using VASP (Vienna Ab initio Simulation Package) code⁴³. The calculations were carried out with the Perdew-Burke-Ernzerhof generalized gradient approximation⁴⁴ density functional, except for the phonon calculation of Zr-H phases with the GGA_PBEsol⁴⁵ functional. The Brillouin zone was sampled using a k-point mesh of $2\pi \times 0.03 \text{ \AA}^{-1}$ for structure relaxations, and a denser spacing of $2\pi \times 0.02 \text{ \AA}^{-1}$ for electronic property calculations. Phonon frequencies and zero point energies were calculated using the supercell approach⁴⁶, as implemented in PHONOPY⁴⁷ and CASTEP codes. The electron-phonon coupling parameters were computed within linear response theory with the Quantum ESPRESSO package⁴⁸; see the Supporting Information for further details.

Acknowledgements

We thank Professor Yanming Ma and Dr. Dmitrii V. Semenov for many interesting and stimulating discussions. This work was supported by the National Key R&D Program of China (No. 2018YFA0305900), National Natural Science Foundation of China (Nos. 51632002 and 11674122), Program for Changjiang Scholars and Innovative Research Team in University (No. IRT_15R23), the 111 Project (No. B12011), and the Natural Sciences and Engineering Research Council of Canada (NSERC). C.J.P. acknowledges financial support from the Engineering and Physical Sciences Research Council (Grant EP/P022596/1) and a Royal Society Wolfson Research Merit award. X. F. acknowledges China Scholarship Council. Parts of the calculations were performed in the High Performance Computing Center (HPCC) of Jilin University and TianHe-1(A) at the National Supercomputer Center in Tianjin.

Author Contributions

D.D. and T.C. designed research; H.X., D.D. and C.J.P. performed calculations; H.X., D.D., C.J.P., V.Z.K., X.F., H.S., S.J., Y.Y. and T.C. analyzed data; H.X., Y.Y., X.F., D.D., Z.Z., S.A.T.R., V.Z.K., C.J.P., and T.C. wrote and revised the paper.

Competing interests

The authors declare no competing interests

References

1. Ashcroft, N. W. Metallic Hydrogen: A High-Temperature Superconductor? *Phys. Rev. Lett.* **21**, 1748-1749 (1968).
2. McMahon, J. M. & Ceperley, D. M. Ground-State Structures of Atomic Metallic Hydrogen. *Phys. Rev. Lett.* **106**, 165302 (2011).
3. Mao, H.-k. & Hemley, R. J. Ultrahigh-pressure transitions in solid hydrogen. *Rev. Mod. Phys.* **66**, 671-692 (1994).
4. Ji, C. et al. Ultrahigh-pressure isostructural electronic transitions in hydrogen. *Nature* **573**, 558-562 (2019).
5. Loubeyre, P., Occelli, F. & Dumas, P. Synchrotron infrared spectroscopic evidence of the probable transition to metal hydrogen. *Nature* **577**, 631-635 (2020).
6. Ashcroft, N. W. Hydrogen dominant metallic alloys: high temperature superconductors? *Phys. Rev. Lett.* **92**, 187002 (2004).
7. Pickard, C. J. & Needs, R. J. High-pressure phases of silane. *Phys. Rev. Lett.* **97**, 045504 (2006).
8. Pickard, C. J. & Needs, R. J. Metallization of aluminum hydride at high pressures: A first-principles study. *Phys. Rev. B* **76**, 144114 (2007).
9. Eremets, M. I., Trojan, I. A., Medvedev, S. A., Tse, J. S. & Yao, Y. Superconductivity in Hydrogen Dominant Materials: Silane. *Science* **319**, 1506 (2008).
10. Duan, D. et al. Pressure-induced metallization of dense $(\text{H}_2\text{S})_2\text{H}_2$ with high- T_c superconductivity. *Sci. Rep.* **4**, 6968 (2014).
11. Drozdov, A. P., Eremets, M. I., Troyan, I. A., Ksenofontov, V. & Shylin, S. I. Conventional superconductivity at 203 kelvin at high pressures in the sulfur hydride system. *Nature* **525**, 73-76 (2015).
12. Einaga, M. et al. Crystal structure of the superconducting phase of sulfur hydride. *Nat. Phys.* **12**, 835 (2016).
13. Huang, X. et al. High-temperature superconductivity in sulfur hydride evidenced by alternating-current magnetic susceptibility. *Natl. Sci. Rev.* **6**, 713-718 (2019).
14. Zhang, S. et al. Phase Diagram and High-Temperature Superconductivity of Compressed Selenium Hydrides. *Sci. Rep.* **5**, 15433 (2015).
15. Liu, H., Naumov, I. I., Hoffmann, R., Ashcroft, N. W. & Hemley, R. J. Potential high- T_c superconducting lanthanum and yttrium hydrides at high pressure. *Proc. Natl. Acad. Sci. U. S. A.* **114**, 6990-6995 (2017).
16. Peng, F. et al. Hydrogen Clathrate Structures in Rare Earth Hydrides at High Pressures: Possible Route to Room-Temperature Superconductivity. *Phys. Rev. Lett.* **119**, 107001 (2017).
17. Geballe, Z. M. et al. Synthesis and Stability of Lanthanum Superhydrides. *Angew. Chem. Int. Ed.* **57**, 688-692 (2018).
18. Drozdov, A. P. et al. Superconductivity at 250 K in lanthanum hydride under high pressures. *Nature* **569**, 528-531 (2019).
19. Somayazulu, M. et al. Evidence for Superconductivity above 260 K in Lanthanum Superhydride at Megabar Pressures. *Phys. Rev. Lett.* **122**, 027001 (2019).
20. Kong, P. et al. Superconductivity up to 243 K in yttrium hydrides under high pressure. *arXiv:1909.10482*, (2019).
21. Kvashnin, A. G., Semenov, D. V., Kruglov, I. A., Wrona, I. A. & Oganov, A. R. High-Temperature Superconductivity in a Th-H System under Pressure Conditions. *ACS Appl. Mater. Interfaces* **10**,

- 43809-43816 (2018).
22. Semenok, D. V. et al. Superconductivity at 161 K in thorium hydride ThH₁₀: Synthesis and properties. *Mater. Today*, <https://doi.org/10.1016/j.mattod.2019.10.005> (2019).
 23. Wang, H., Tse, J. S., Tanaka, K., Iitaka, T. & Ma, Y. Superconductive sodalite-like clathrate calcium hydride at high pressures. *Proc. Natl. Acad. Sci. U. S. A.* **109**, 6463 (2012).
 24. Pickard, C. J., Martinez-Canales, M. & Needs, R. J. Density functional theory study of phase IV of solid hydrogen. *Phys. Rev. B* **85**, 214114 (2012).
 25. Pickard, C. J. & Needs, R. J. Structure of phase III of solid hydrogen. *Nat. Phys.* **3**, 473-476 (2007).
 26. Howie, R. T., Guillaume, C. L., Scheler, T., Goncharov, A. F. & Gregoryanz, E. Mixed molecular and atomic phase of dense hydrogen. *Phys. Rev. Lett.* **108**, 125501 (2012).
 27. Pépin, C. M., Geneste, G., Dewaele, A., Mezouar, M. & Loubeyre, P. Synthesis of FeH₅: A layered structure with atomic hydrogen slabs. *Science* **357**, 382 (2017).
 28. Zhong, X. et al. Tellurium Hydrides at High Pressures: High-Temperature Superconductors. *Phys. Rev. Lett.* **116**, 057002 (2016).
 29. Zhou, D. et al. *Ab initio* study revealing a layered structure in hydrogen-rich KH₆ under high pressure. *Phys. Rev. B* **86**, 014118 (2012).
 30. Liu, Y. et al. First-principles study on the structural and electronic properties of metallic HfH₂ under pressure. *Sci. Rep.* **5**, 11381 (2015).
 31. Kuzovnikov, M. A. & Tkacz, M. High-Pressure Synthesis of Novel Polyhydrides of Zr and Hf with Th₄H₁₅-type Structure. *J. Phys. Chem. C* **123**, 30059–30066 (2019).
 32. Xia, H., Parthasarathy, G., Luo, H., Vohra, Y. K. & Ruoff, A. L. Crystal structures of group IVa metals at ultrahigh pressures. *Phys. Rev. B* **42**, 6736-6738 (1990).
 33. Labet, V., Gonzalez-Morelos, P., Hoffmann, R. & Ashcroft, N. W. A fresh look at dense hydrogen under pressure. I. An introduction to the problem, and an index probing equalization of H–H distances. *J. Chem. Phys.* **136**, 074501 (2012).
 34. Wu, Y., Lazic, P., Hautier, G., Persson, K. & Ceder, G. First principles high throughput screening of oxynitrides for water-splitting photocatalysts. *Energy Environ. Sci.* **6**, 157-168 (2013).
 35. Allen, P. B. & Dynes, R. C. Transition temperature of strong-coupled superconductors reanalyzed. *Phys. Rev. B* **12**, 905-922 (1975).
 36. Gor'kov, L. P. & Kresin, V. Z. Colloquium: High pressure and road to room temperature superconductivity. *Rev. Mod. Phys.* **90**, 011001 (2018).
 37. Ye, X., Zarifi, N., Zurek, E., Hoffmann, R. & Ashcroft, N. W. High Hydrides of Scandium under Pressure: Potential Superconductors. *J. Phys. Chem. C* **122**, 6298-6309 (2018).
 38. Pickard, C. J. & Needs, R. J. *Ab initio* random structure searching. *J. Phys.: Condens. Matter* **23**, 053201 (2011).
 39. Wang, Y., Lv, J., Zhu, L. & Ma, Y. Crystal structure prediction via particle-swarm optimization. *Phys. Rev. B* **82**, 094116 (2010).
 40. Oganov, A. R. & Glass, C. W. Crystal structure prediction using *ab initio* evolutionary techniques: Principles and applications. *J. Chem. Phys.* **124**, 244704 (2006).
 41. Segall, M. D. et al. First-principles simulation: ideas, illustrations and the CASTEP code. *J. Phys.: Condens. Matter* **14**, 2717 (2002).
 42. Kresse, G. & Joubert, D. From ultrasoft pseudopotentials to the projector augmented-wave method. *Phys. Rev. B* **59**, 1758-1775 (1999).
 43. Kresse, G. & Furthmüller, J. Efficiency of *ab-initio* total energy calculations for metals and

- semiconductors using a plane-wave basis set. *Comput. Mater. Sci.* **6**, 15-50 (1996).
44. Perdew, J. P., Burke, K. & Ernzerhof, M. Generalized Gradient Approximation Made Simple. *Phys. Rev. Lett.* **77**, 3865-3868 (1996).
45. Perdew, J. P. et al. Restoring the Density-Gradient Expansion for Exchange in Solids and Surfaces. *Phys. Rev. Lett.* **100**, 136406 (2008).
46. Parlinski, K., Li, Z. Q. & Kawazoe, Y. First-Principles Determination of the Soft Mode in Cubic ZrO_2 . *Phys. Rev. Lett.* **78**, 4063-4066 (1997).
47. Togo, A., Oba, F. & Tanaka, I. First-principles calculations of the ferroelastic transition between rutile-type and CaCl_2 -type SiO_2 at high pressures. *Phys. Rev. B* **78**, 134106 (2008).
48. Paolo, G. et al. QUANTUM ESPRESSO: a modular and open-source software project for quantum simulations of materials. *J. Phys.: Condens. Matter* **21**, 395502 (2009).

Supporting Information

For

Hydrogen “penta-graphene-like” structure stabilized by hafnium: high-temperature conventional superconductor

Hui Xie¹, Yansun Yao², Xiaolei Feng^{3,4}, Defang Duan^{1,5,*}, Hao Song¹, Zihan Zhang¹, Shuqing Jiang¹,
Simon A. T. Redfern⁶, Vladimir Z. Kresin⁷, Chris J. Pickard^{5,8,*} and Tian Cui^{9,1,*}

¹*State Key Laboratory of Superhard Materials, college of Physics, Jilin University, Changchun 130012, China*

²*Department of Physics and Engineering Physics, University of Saskatchewan, Saskatoon, Saskatchewan S7N 5E2, Canada*

³*Center for High Pressure Science and Technology Advanced Research, Beijing 100094, China*

⁴*Department of Earth Science, University of Cambridge, Downing Site, Cambridge CB2 3EQ, United Kingdom*

⁵*Department of Materials Science & Metallurgy, University of Cambridge, 27 Charles Babbage Road, Cambridge CB3 0FS, United Kingdom*

⁶*Asian School of the Environment, Nanyang Technological University, Singapore 639798*

⁷*Lawrence Berkeley Laboratory, University of California at Berkeley, Berkeley, CA 94720, USA*

⁸*Advanced Institute for Materials Research, Tohoku University 2-1-1 Katahira, Aoba, Sendai, 980-8577, Japan*

⁹*School of Physical Science and Technology, Ningbo University, Ningbo, 315211, People's Republic of China*

*Corresponding authors email: duandf@jlu.edu.cn, cjp20@cam.ac.uk, cuitian@jlu.edu.cn

Content

| | |
|--|-----|
| Computational details..... | S3 |
| Equations for calculating T_c and related parameters..... | S4 |
| Comparison of high T_c hydrides families | S8 |
| Thermodynamic stability of Hf-H system..... | S9 |
| Structures and bond analysis of Hf-H system..... | S10 |
| Thermodynamic stability of Zr-H system | S12 |
| Superconductive parameters of MH_{10} (M=Hf, Zr, Sc and Lu)..... | S13 |
| Projected DOS and superconductive parameters of the other hafnium hydrides | S14 |
| MgH_{10} and ThH_{10} | S16 |
| ScH_{10} | S16 |
| LuH_{10} | S18 |
| Dynamic stability | S20 |
| EOS for MH_3 (M=Hf, Zr and Lu)..... | S22 |
| Structural information | S24 |
| References | S26 |

Computational details

High-pressure structural predictions within *ab initio* calculations are implemented with the AIRSS (Ab Initio Random Structure Searching) code¹, which effectiveness has been confirmed by the successful applications to discovering the structures of solids, point defects, surfaces, and clusters. CALYPSO (Crystal structure AnaLYsis by Particle Swarm Optimization)²⁻³ and USPEX (Universal Structure Predictor: Evolutionary Xtallography)⁴⁻⁶ codes were also used for searching high-pressure structures of Zr-H system, giving the same results as that generated by using AIRSS.

Given that most of the recently discovered superconducting superhydrides are stable at pressures above 100 GPa, some even at pressures higher than 300 GPa, we set our initial structure searches at 300 GPa. Extensive random structure searches were carried out for 40 compositions which resulted in the generation of approximately 15,000 structures, among which HfH₂₄ showed the highest hydrogen content. A convex hull was constructed for each predicted compounds and those laying on or within ~ 0.1 eV/atom above the convex hull were selected for refined structural optimization with higher criteria (Fig. S1). As shown in Fig. S1 (a), the structure searches have identified an extremely H-rich species of HfH₁₈ with general accuracy, while it loses its stability in high precision calculations, as shown in Fig S1 (b). For all thermodynamically stable stoichiometries (those on the convex hull), HfH₁₀ showed the highest hydrogen content. Subsequently, fixed-composition searches were carried out restricting the Hf:H ratio to (or below) 1:10, *i.e.*, HfH_{*x*} (*x*=1-10), and these were performed at 100, 200 and 300 GPa.

For Hf-H and Zr-H systems, structural relaxations were performed by the on-the-fly (OTF) generation of ultrasoft pseudopotentials in CASTEP (Cambridge Sequential Total Energy Package) code⁷, where the valence electrons configurations are $4f^{14}5s^25p^65d^26s^2$ for Hf, $4s^24p^64d^25s^2$ for Zr and $1s^1$ for H. The cutoff energy was chosen to be 800 eV. In other cases, the all-electron projector-augmented wave method (PAW)⁸ pseudopotentials were employed using VASP code⁹ with cutoff energy of 1000 eV. The valence electrons of the pseudopotentials are $3p^63d^14s^2$ for Sc, $4f^{14}5s^25p^65d^16s^2$ for Lu, $2s^22p^63s^2$ for Mg, $6p^66d^27s^2$ for Th and $1s^1$ for H. The exchange-correlation functional was described using Perdew–Burke–Ernzerhof (PBE) of generalized gradient approximation (GGA)¹⁰⁻¹¹ for all systems. A Monkhorst-Pack¹² k-point mesh of $2\pi \times 0.03 \text{ \AA}^{-1}$ was used to ensure that the enthalpy calculations converged effectively to within less than 1 meV/atom.

All-electron full-potential linearized augmented plane wave (FP-LAPW) method with WIEN2k

code¹³ was performed to test the validity of the PAW pseudopotentials used in VASP and OTF pseudopotentials used in CASTEP. In the full-potential calculations, the FP-LAPW basis function of RKmax = 5 and 3000 k points in the electronic integration of the Brillouin zone were used to achieve a satisfactory degree of convergence. The Perdew-Burke-Ernzerhof generalized gradient approximation (GGA_PBE) exchange correlation functional was chosen. The pressure-volume curves of MH₃ were fitted by third-order Birch-Murnaghan (BM) equation¹⁴.

Electronic properties were calculated by means of the VASP code using a k-point mesh of $2\pi \times 0.02 \text{ \AA}^{-1}$. Electron localization function (ELF)¹⁵ was computed to describe and visualize chemical bonds in multielectron systems, which can easily reveal atomic shell structure and core, binding, and lone electron pairs. The ELF value is in the range of 0-1. The upper limit ELF = 1 corresponds to perfect localization and the value ELF = 0.5 corresponds to electron gas-like pair probability. The crystal orbital Hamiltonian population (COHP) and integrated COHP (ICOHP) were also calculated using LOBSTER¹⁶, which is commonly used for differentiating covalent and non-covalent bonding in chemistry. And Bader charge analysis¹⁷⁻¹⁸ was performed to determine charge transfer.

The phonon and zero point energy calculations were carried out using the PHONOPY¹⁹ and CASTEP codes. In the calculations, GGA_PBE and GGA_PBEsol²⁰ exchange correlation functional were chosen for Hf-H and Zr-H systems, respectively. The linear response theory was performed to calculate the electron-phonon coupling (EPC) with the Quantum ESPRESSO package²¹. Convergence tests gave us an appropriate kinetic energy cutoff of 90 Ry. Pseudopotentials were generated by a Troullier-Martins norm-conserving scheme²² which is found to be particular efficient for systems containing first-row elements and transition metals. Self-consistent electron density and electron-phonon coupling were calculated by employing 12×12×18 k-mesh and 4×4×6 q-mesh for *P*6₃/*mmc*-MH₁₀ (M = Hf, Zr, Sc and Lu). The superconducting transition temperatures T_c were calculated using three different equations as follows²³⁻²⁶.

Equations for calculating T_c and related parameters

In this section we will introduce the equations for calculating T_c of hydrides. The metallic hydrides which possess high T_c were considered as conventional superconductors (the pairing mechanism is the electron-phonon interaction). And the high T_c is mainly attributed to the motion of H atoms. In order to study influence of the forms (cages, penta-graphene-like and covalent

compound) of H -structures in hydrides on T_c , we analyse as the dominant the contribution of optical modes, because of large difference in masses. Indeed, as we know, the optical modes are determined by the hydrogen motion, whereas the acoustic modes correspond to the motion of heavy ion.

The Eliashberg equation for the pairing order parameter $\Delta(\omega_j)$ has the following form (at $T = T_c$)²³:

$$\Delta(\omega_j)Z = \pi T_c \sum_i \int d\omega \frac{\alpha^2(\omega)F(\omega)}{\omega} \frac{\omega^2}{\omega^2 + (\omega_j - \omega_i)^2} \frac{\Delta\omega_i}{|\omega_i|}. \quad (S1)$$

Here, Z is the renormalization factor:

$$Z = 1 + \frac{\pi T_c}{\omega_j} \sum_i \int d\omega \frac{\alpha^2(\omega)F(\omega)}{\omega} \frac{\omega^2}{\omega^2 + (\omega_j - \omega_i)^2} \frac{\omega_i}{|\omega_i|}. \quad (S1)$$

And ω_i is the Matsubara frequency:

$$\omega_i = (2i + 1)\pi T_c \quad (i = 0, \pm 1, \pm 2, \dots), \quad (S3)$$

In our calculations, the cut off Matsubara frequency is $|i| \leq 24$ (when $|i_{max}| = 24$., $\omega_{max} \approx 300$ THz for the $T_c \approx 200$ K). The Eliashberg equation is a non-linear integral equation. Here we used the Matsubara-type linearized Eliashberg equations, introduced by Bergmann and Rainer²⁷⁻²⁸ and Allen²⁹, and later developed by Kvashin et al.³⁰, to get the approximate solution of the Eliashberg equation (LE):

$$\Delta(\omega = \omega_j, T) = \Delta_i(T) = \pi T \sum_i \frac{[\lambda(\omega_j - \omega_i) - \mu^*]}{\rho + |\omega_i + \pi T \sum_k (\text{sign} \omega_k) \cdot \lambda(\omega_i - \omega_k)|} \cdot \Delta_i(T), \quad (S4)$$

where μ^* is a Coloumb pseudopotential. The function $\lambda(\omega_j - \omega_i)$ relates to effective electron-electron interaction via exchange of phonons and takes forms:

$$\lambda(\omega_j - \omega_i) = 2 \int_0^\infty \frac{\omega \cdot \alpha^2 F(\omega)}{\omega^2 + (\omega_j - \omega_i)^2} d\omega. \quad (S5)$$

Transition temperature T_c can be found as a solution of equation $\rho(T_c) = 0$, where $\rho(T)$ is defined as $\max(\rho)$ providing that $\Delta(\omega)$ is not a zero function of ω at fixed temperature. Here provided a way to calculate $\rho(T)$:

$$\rho(T) = \max\{\text{eigenvalue}(K_{mn})\}e, \quad (S6)$$

$$K_{mn} = F(m - n) + F(m + n + 1) - 2\mu^* - \delta_{mn}[2m + 1 + F(0) + 2 \sum_{l=1}^m F(l)], \quad (S7)$$

$$F(n) = F(n, T) = 2 \int_0^{\omega_{max}} \frac{\alpha^2 F(\omega)}{\omega^2 + (2\pi \cdot T \cdot n)^2} \cdot \omega d\omega. \quad (S8)$$

Here, the $\rho(T) = 0$ when $T = T_c$.

The EPC spectral function $\alpha^2 F(\omega)$ is given by²⁴:

$$\alpha^2 F(\omega) = \frac{1}{2\pi N(\epsilon_f)} \sum_{qj} \frac{\gamma_{qj}}{\omega_{qj}} \delta(\omega - \omega_{qj}) w(q). \quad (S9)$$

γ_{qj} is the phonon linewidth,

$$\gamma_{qj} = 2\pi\omega_{qj} \sum_{nm} \int \frac{d^3k}{\Omega_{BZ}} |g_{kn,k+qm}^j|^2 \delta(\varepsilon_{kn} - \varepsilon_F) \delta(\varepsilon_{k+qm} - \varepsilon_F), \quad (\text{S10})$$

where Ω_{BZ} is the volume of the BZ, $g_{kn,k+qm}^j$ are the electron-phonon matrix elements, ε_F is the Fermi energy, ε_{kn} and ε_{k+qm} are the Kohn-Sham eigenvalues in the band n at wave vector k and band m at wave vector $k + q$, respectively.

The Allen-Dynes modified McMillan equation (A-D) which is the approximate analytic solution of the Eliashberg equations valid at $\lambda < 1.5$ is²⁴:

$$T_c = \frac{\omega_{log}}{1.2} \exp \left[-\frac{1.04(1+\lambda)}{\lambda - \mu^*(1+0.62\lambda)} \right], \quad (\text{S11})$$

when $\lambda > 1.5$, we have the following expression containing the corrections f_1 and f_2 ::

$$T_c = \frac{f_1 f_2 \omega_{log}}{1.2} \exp \left[-\frac{1.04(1+\lambda)}{\lambda - \mu^*(1+0.62\lambda)} \right], \quad (\text{S12})$$

two separate correction factors f_1 and f_2 are given by²⁴:

$$f_1 = \sqrt[3]{1 + \left(\frac{\lambda}{2.46(1+3.8\mu^*)} \right)^2}, f_2 = 1 + \frac{(\bar{\omega}_2 - 1)\lambda^2}{\lambda^2 + [1.82(1+6.3\mu^*)\frac{\bar{\omega}_2}{\omega_{log}}]^2}, \quad (\text{S13})$$

Here $\bar{\omega}_2$ is mean square frequency,

$$\bar{\omega}_2 = \sqrt{\frac{2}{\lambda} \int \alpha^2 F(\omega) \omega d\omega}, \quad (\text{S14})$$

ω_{log} is the logarithmic average frequency and μ^* is the Coulomb pseudopotential, for which we use the widely accepted range of 0.1-0.13. The ω_{log} and EPC constant λ were calculated as:

$$\omega_{log} = \exp \left[\frac{2}{\lambda} \int \frac{d\omega}{\omega} \alpha^2 F(\omega) \ln \omega \right], \quad (\text{S15})$$

$$\lambda = 2 \int \frac{\alpha^2 F(\omega)}{\omega} d\omega = \sum_{qj} \lambda_{qj} w(q), \quad (\text{S16})$$

$$\lambda_{qj} = \frac{\gamma_{qj}}{\pi \hbar N(\varepsilon_F) \omega_{qj}^2}, \quad (\text{S17})$$

where λ_{qj} is the mode EPC parameter³¹ and $w(q)$ is the weight of phonon mode j at wave vector q in the first Brillouin zone (BZ).

The phonon spectrum of hydrides contains acoustic and optical modes and is very broad because of the presence of light hydrogen ions. In order to study the impact of H atoms, Gor'kov and Kresin (G-K) introduced the coupling constants λ_{opt} and λ_{ac} describing the interaction of electrons with optical and acoustic phonons, respectively²⁵⁻²⁶.

$$\lambda_{ac} = 2 \int_0^{\omega_1} \frac{\alpha^2 F(\omega)}{\omega} d\omega, \lambda_{opt} = 2 \int_{\omega_1}^{\omega_m} \frac{\alpha^2 F(\omega)}{\omega} d\omega, \lambda_{ac} + \lambda_{opt} = \lambda, \quad (\text{S18})$$

where ω_1 is the maximum frequency for the acoustic modes, ω_m is the maximum value of frequency of the optical modes. The average values are defined as follows:

$$\tilde{\omega}_{ac} = \langle \omega_{ac}^2 \rangle^{\frac{1}{2}}, \quad \langle \omega_{ac}^2 \rangle = \frac{2}{\lambda_{ac}} \int_0^{\omega_1} d\omega \cdot \omega^2 \frac{\alpha^2 F(\omega)}{\omega} = \frac{2}{\lambda_{ac}} \int_0^{\omega_1} \alpha^2 F(\omega) \omega d\omega, \quad (S19)$$

$$\tilde{\omega}_{opt} = \langle \omega_{opt}^2 \rangle^{\frac{1}{2}}, \quad \langle \omega_{opt}^2 \rangle = \frac{2}{\lambda_{opt}} \int_{\omega_1}^{\omega_m} d\omega \cdot \omega^2 \frac{\alpha^2 F(\omega)}{\omega} = \frac{2}{\lambda_{opt}} \int_{\omega_1}^{\omega_m} \alpha^2 F(\omega) \omega d\omega, \quad (S20)$$

Then the generalized Eliashberg equation has the form:

$$\Delta(\omega_n)Z = \pi T \sum_{\omega_{n'}} \left[\lambda_{opt} \frac{\tilde{\Omega}_{opt}^2}{\tilde{\Omega}_{opt}^2 + (\omega_n - \omega_{n'})^2} + \lambda_{ac} \frac{\tilde{\Omega}_{ac}^2}{\tilde{\Omega}_{ac}^2 + (\omega_n - \omega_{n'})^2} \right] \frac{\Delta(\omega_{n'})}{|\omega_{n'}|} \Big|_{T=T_c}, \quad (S21)$$

For our predicted hydrides the $\lambda_{ac} \ll \lambda_{opt}$, we assume that:

$$T_c = T_c^{opt} + \Delta T_c^{ac}, \text{ and } T_c^{opt} \gg \Delta T_c^{ac} \quad (S22)$$

As a result, the expression for T_c can be written in the form:

$$T_c = \left[1 + 2 \frac{\lambda_{ac}}{\lambda_{opt} - \mu^*} \cdot \frac{1}{1 + \eta^{-2}} \right] T_c^0, \quad \eta = \frac{\tilde{\omega}_{ac}}{\pi T_c^0}, \quad T_c^0 \equiv T_c^{opt}. \quad (S23)$$

Here the T_c^0 is defined as the transition temperatures caused by the interaction of electrons with optical phonons only, for $\lambda_{opt} \gtrsim 1.5$:

$$T_c^0 = \frac{\tilde{\omega}_{opt}}{1.2} \exp \left[- \frac{1.04(1 + \lambda_{opt})}{\lambda_{opt} - \mu^* (1 + 0.62 \lambda_{opt})} \right]. \quad (S24)$$

For $\lambda_{opt} > 1.5$:

$$T_c^0 = \frac{0.25 \tilde{\omega}_{opt}}{[e^{\frac{2}{\lambda_{eff}}} - 1]^{1/2}}. \quad (S25)$$

Here the λ_{eff} is defined as follows:

$$\lambda_{eff} = (\lambda_{opt} - \mu^*) [1 + 2\mu^* + \lambda_{opt}\mu^* t(\lambda_{opt})]^{-1}, \quad (S26)$$

$$t(x) = 1.5 \exp(-0.28) x. \quad (S27)$$

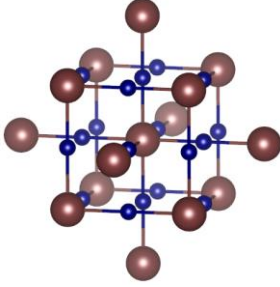
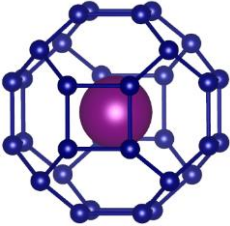
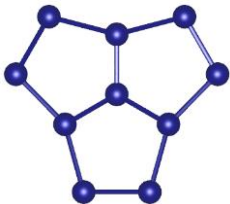
The values of the isotope coefficient α and superconductive gap were calculated with use of the following expressions:

$$\alpha = \frac{1}{2} \left[1 - 4 \frac{\lambda_{ac}}{\lambda_{opt}} \frac{\eta^2}{(\eta^2 + 1)^2} \right], \quad (S28)$$

$$\frac{2\Delta(0)}{T_c} = 3.52 \left[1 + 5.3 \left(\frac{T_c}{\tilde{\omega}} \right)^2 \ln \frac{\tilde{\omega}}{T_c} \right]. \quad (S29)$$

Comparison of high T_c hydrides families

Table S1. Comparison of three families of binary hydrides with high T_c .

| hydrogenic motifs | Hydrides (atomic radius/ electronegativity) Electronic configuration | Symmetry | T_c , K (P, GPa) |
|--|--|--------------|--|
|  H-S(Se) covalent bond | H_3S (1.84 Å / 2.58) [Ne] 3s ² 3p ⁴ | $Im\bar{3}m$ | 204 ^a (200) ³² 203 ^b (155) ³³ |
| | H_3Se (1.98 Å / 2.55) [Ne] 3d ¹⁰ 4s ² 4p ⁴ | | 110 ^a (200) ³⁴ |
|  H ₃₂ cage | LaH_{10} (1.88 Å / 1.10) [Xe] 5d ¹ 6s ² | $Fm\bar{3}m$ | 288 ^a (200) ³⁵ 250-260 ^b (170-200) ³⁶⁻³⁷ |
| | YH_{10} (1.81 Å / 1.22) [Kr] 4d ¹ 5s ² | | 303 ^a (400) ³⁵ |
| | ThH_{10} (1.80 Å / 1.30) [Rn] 6d ² 7s ² | | 241 ^a (100) ³⁸ 161 ^b (174) ³⁹ |
|  H ₁₀ penta-graphene ^c | HfH_{10} (1.56 Å / 1.30) [Xe] 4f ¹⁴ 5d ² 6s ² | $P6_3/mmc$ | 234 (250) |
| | ZrH_{10} (1.60 Å / 1.33) [Kr] 4d ² 5s ² | | 220 (250) |
| | ScH_{10} (1.61 Å / 1.36) [Ar] 3d ¹ 4s ² | | 158 (250) |
| | LuH_{10} (1.73 Å / 1.27) [Xe] 4f ¹⁴ 5d ¹ 6s ² | | 152 (200) |

^a T_c values were calculated with $\mu^* = 0.1$.

^b T_c was measured experimentally.

^c T_c values were calculated with G-K equation at $\mu^* = 0.1$.

Thermodynamic stability of Hf-H system

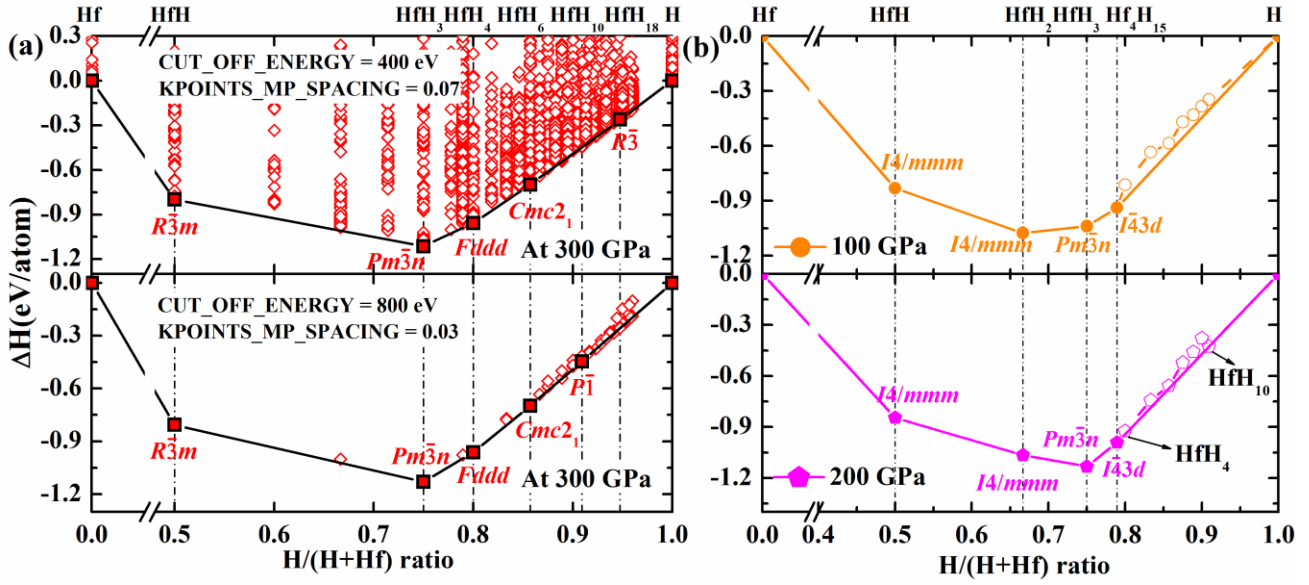


Fig. S1 (a) Predicted formation enthalpies of Hf-H system barring ZPEs with general (upper panel) and high accuracy (nether panel) at 300 GPa. (b) Formation enthalpies of HfH_x (x=1-10) not inclusion ZPE with high accuracy at 100 and 200 GPa. Here, the compounds on the convex hull are thermodynamically stable and, in principle, experimentally synthesizable under corresponding pressures. As can be seen, HfH is predicted to be stable with $I4/mmm$ symmetry from 100 GPa to 200 GPa, then transforms into $R\bar{3}m$ at 300 GPa. HfH₂ adopts the $I4/mmm$ structure between 100 GPa and 200 GPa, and then breaks down with respect to a mixture of Hf and HfH₃ at 300 GPa. HfH₃ is stabilized in a $Pm\bar{3}n$ structure at 100 GPa, and remains as such up to at least 300 GPa. Hf₄H₁₅ is predicted to be stable below 200 GPa with space group of $I\bar{4}3d$. $Fddd$ -HfH₄, $Cmc2_1$ -HfH₆ and $P\bar{1}$ -HfH₁₀ are only stable at 300 GPa.

Table S2. Calculated enthalpies and ZPE values of $P\bar{1}$ and $P6_3/mmc$ of HfH_{10} at different pressures. Numbers between parentheses represent the atoms in the supercells using different softwares (VASP/CASTEP).

| Phase (HfH_{10}) | P (GPa) | Enthalpy (eV/f.u.) | | ZPE (eV/f.u.) | | Enthalpy + ZPE (eV/f.u.) | |
|---|------------|--------------------|------------|---------------|--------|--------------------------|------------|
| | | VASP | CASTEP | VASP | CASTEP | VASP | CASTEP |
| $P\bar{1}$ (88/88) | 200 | 1.3108 | -7977.4660 | 2.9915 | 3.0468 | 4.3023 | -7974.4192 |
| | 250 | 9.8058 | -7968.9748 | 3.1177 | 3.1697 | 12.9235 | -7965.8051 |
| | 300 | 17.7743 | -7961.0109 | 3.2245 | 3.2779 | 20.9988 | -7957.7330 |
| $P6_3/mmc$ (66/44) | 200 | 1.9724 | -7976.7688 | 2.5059 | 2.5712 | 4.4783 | -7974.1976 |
| | 250 | 10.2612 | -7968.4730 | 2.7255 | 2.7245 | 12.9867 | -7965.7485 |
| | 300 | 18.0640 | -7960.6644 | 2.9132 | 2.8890 | 20.9772 | -7957.7754 |
| ΔE [$P\bar{1}$ - $P6_3/mmc$] | 200 | -0.6616 | -0.6972 | 0.4856 | 0.4756 | -0.1760 | -0.2216 |
| | 250 | -0.4554 | -0.5018 | 0.3922 | 0.4452 | -0.0632 | -0.0566 |
| | 300 | -0.2897 | -0.3465 | 0.3113 | 0.3889 | 0.0216 | 0.0424 |

Structures and bond analysis of Hf-H system

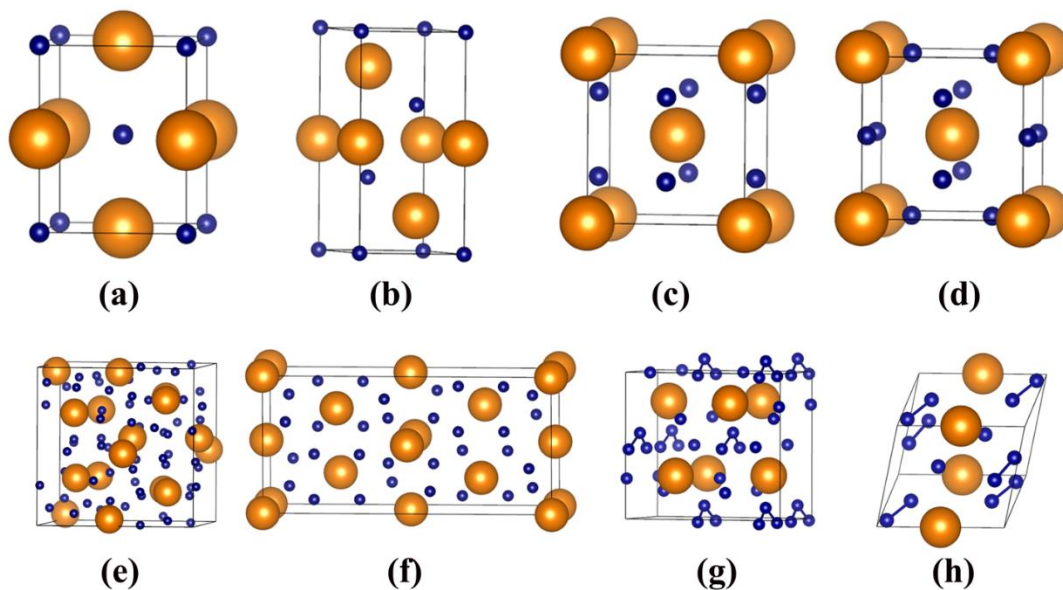


Fig. S2. Structures of stable Hf-H compounds under high pressures. (a) $I4/mmm$ in HfH , (b) $R\bar{3}m$ in HfH , (c) $I4/mmm$ in HfH_2 , (d) $Pm\bar{3}n$ in HfH_3 , (e) $R\bar{3}c$ in HfH_3 , (f) $I\bar{4}3d$ in Hf_4H_{15} , (g) $Fddd$ in HfH_4 (h) $Cmc2_1$ in HfH_6 , (i) $P\bar{1}$ in HfH_{10} . Large golden spheres denote Hf atoms, while the small blue spheres represent H atoms.

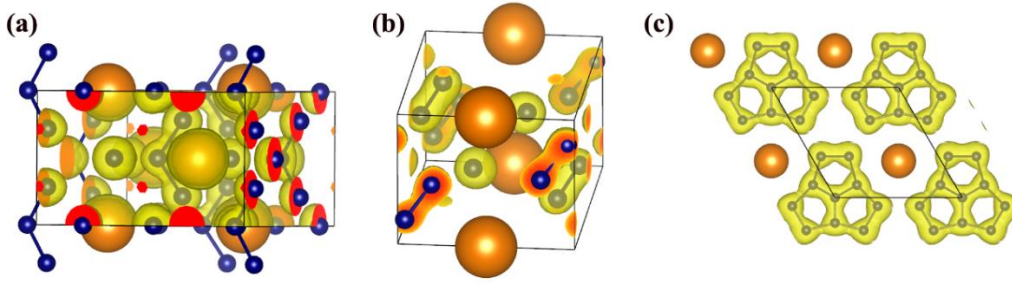


Fig. S3. The calculated ELF of (a) *Cmc*2₁-HfH₆ with isosurface value of 0.7 at 300 GPa, (b) *P*1̄-HfH₁₀ with isosurface value of 0.8 at 200 GPa, (c) *P*6₃/*mmc*-HfH₁₀ with isosurface value of 0.6 at 300 GPa. For HfH₆, The H-H bond lengths in the H₃ unit are approximately 0.97 Å and 1.05 Å at 300 GPa. The electron localization function (ELF) values of the H-H bonds in HfH₆ reach 0.7-0.8, indicating strong covalent bonding characteristics. The *P*1̄ structure of HfH₁₀ consists of diatomic hydrogen pairs similar to H₂ molecules in which the H-H distances are 0.84 and 0.91 Å and ELF values greater than 0.8 at 200 GPa, which also corresponds to strong covalent bonding.

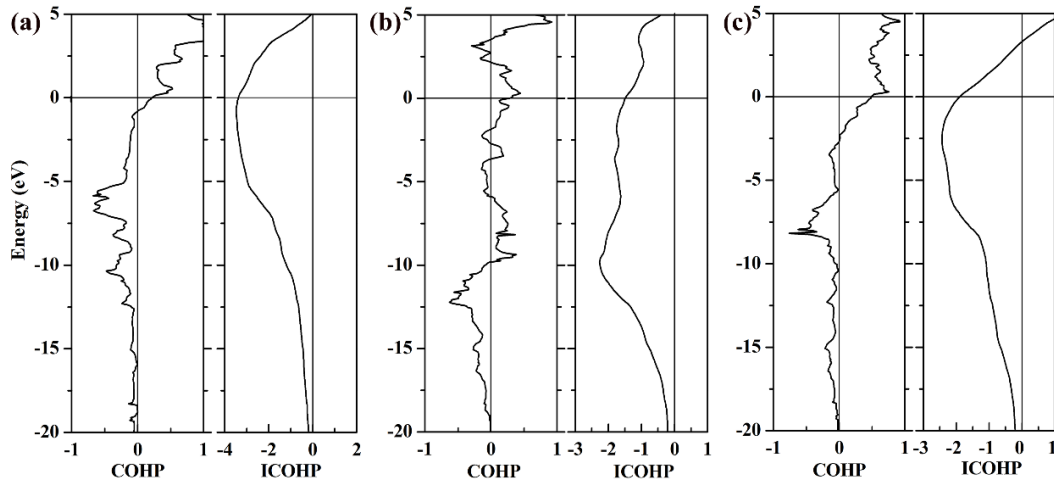


Fig. S4. The calculated Crystalline Orbital Hamiltonian Population (COHP) and Integrated Crystalline Orbital Hamiltonian Population (ICOHP) of *P*6₃/*mmc*-HfH₁₀ with H-H distances of (a) 0.92, (b) 1.02 and (c) 1.07 Å at 300 GPa. The horizontal lines present the Fermi levels. The negative COHP indicates bonding and positive COHP indicates antibonding. And the negative ICOHP values represent the bonding interactions between the H atoms. The fully occupied bonding states and partially occupied antibonding states lend a strong support on the H-H covalent bonding within the planar H₁₀ units.

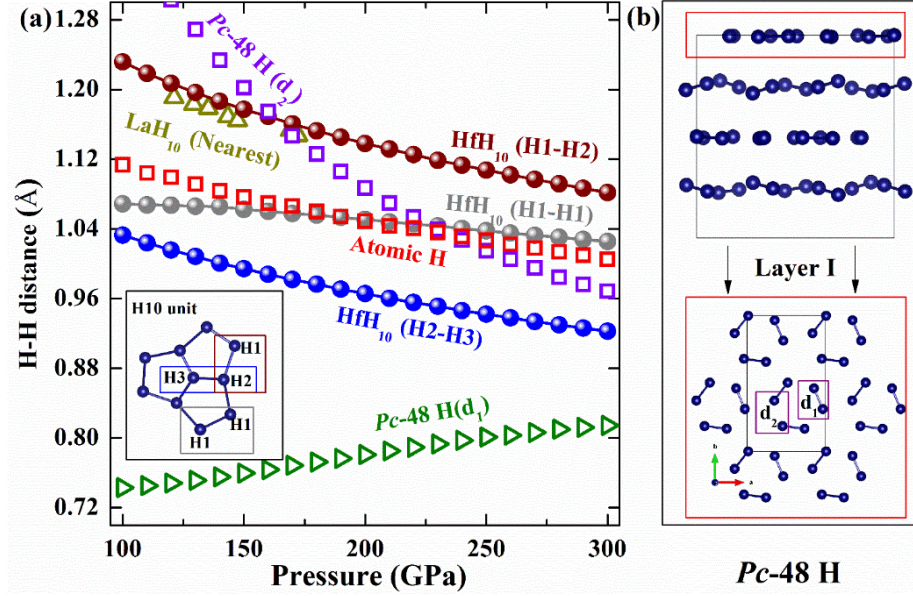


Fig. S5. (a) The calculated H-H distances in HfH_{10} in comparison to LaH_{10} , atomic H and $Pc-48\text{ H}$ in a pressure range of 100-300 GPa. Inset: schematic diagram of H_{10} unit in HfH_{10} . (b) Side view of the $Pc-48\text{ H}$ structure and top view of a weakly bonded graphene-like layer (layer I).

Thermodynamic stability of Zr-H system

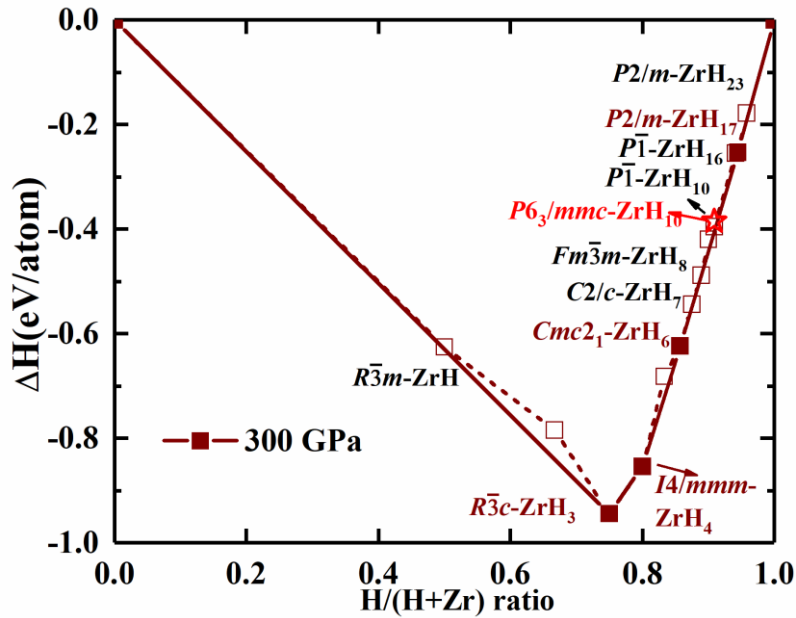


Fig. S6. Predicted formation enthalpies of Zr-H system with decomposition into elemental zirconium and hydrogen at 300 GPa. It is found that ZrH_3 , ZrH_4 , ZrH_6 and ZrH_{17} are thermodynamically stable, while ZrH_{10} is metastable. For ZrH_{10} , $P6_3/mmc$ and $P\bar{1}$ phases are competitive phase with 18 meV/atom and 8 meV/atom above the convex hull, respectively.

Table S3. Calculated enthalpies and ZPE values of ZrH₁₀ structures. Numbers between parentheses represent the atoms in the supercells using different softwares (VASP/CASTEP).

| Phase (ZrH ₁₀) | P (GPa) | Enthalpy (eV/f.u.) | | ZPE (eV/f.u.) | | Enthalpy + ZPE (eV/f.u.) | |
|---|------------|--------------------|------------|---------------|--------|--------------------------|------------|
| | | VASP | CASTEP | VASP | CASTEP | VASP | CASTEP |
| $P\bar{1}$ (88/44) | 200 | 5.8245 | -1403.6864 | 2.7388 | 2.8256 | 8.5633 | -1400.8608 |
| | 250 | 14.2116 | -1395.3404 | 2.8666 | 2.9478 | 17.0782 | -1392.3926 |
| | 300 | 22.0854 | -1387.5206 | 2.9863 | 3.0713 | 25.0717 | -1384.4493 |
| $P6_3/mmc$ (66/44) | 200 | 5.9177 | -1403.5396 | 2.5975 | 2.6115 | 8.5152 | -1400.9281 |
| | 250 | 14.2794 | -1395.2253 | 2.7879 | 2.8030 | 17.0673 | -1392.4223 |
| | 300 | 22.1523 | -1387.4095 | 2.9397 | 2.9316 | 25.0920 | -1384.4779 |
| ΔE [$P\bar{1}$ - $P6_3/mmc$] | 200 | -0.0932 | -0.1468 | 0.1413 | 0.2141 | 0.0481 | 0.0673 |
| | 250 | -0.0678 | -0.1151 | 0.0787 | 0.1448 | 0.0109 | 0.0297 |
| | 300 | -0.0669 | -0.1111 | 0.0466 | 0.1397 | -0.0203 | 0.0286 |

Superconductive parameters of MH₁₀ (M=Hf, Zr, Sc and Lu)

Table S4. The calculated EPC parameter λ , logarithmic average phonon frequency ω_{log} (K), electronic density of states at Fermi level $N(\epsilon_f)$ (states/spin/Ry/f.u.) and superconducting transition temperatures T_c (K) with $\mu^* = 0.1-0.13$ at corresponding pressures P (GPa).

| Structure | P | λ | ω_{log} | $N(\epsilon_f)$ | T_c (K) ^a | A-D T_c (K) ^b | LE T_c (K) | G-K T_c (K) |
|---------------------------------|-----|-----------|----------------|-----------------|------------------------|-------------------------------|-----------------|------------------|
| $P6_3/mmc$ -HfH ₁₀ | 250 | 2.77 | 677.3 | 6.5 | 112-118 | 152-167 | 226-239 | 213-234 |
| | 300 | 2.16 | 861.5 | 6.2 | 122-130 | 151-166 | 214-228 | 197-220 |
| $P6_3/mmc$ -ZrH ₁₀ | 250 | 1.77 | 1068.8 | 6.4 | 130-141 | 151-167 | 185-198 | 199-220 |
| | 300 | 1.59 | 1162.6 | 6.1 | 128-140 | 145-162 | 177-191 | 194-218 |
| $P6_3/mmc$ -ScH ₁₀ | 250 | 1.16 | 1211.3 | 3.6 | 92-104 | 99-114 | 112-124 | 134-158 |
| $P6_3/mmc$ -LuH ₁₀ | 200 | 1.36 | 1024.2 | 3.4 | 95-105 | 105-118 | 123-134 | 134-152 |
| $Fm\bar{3}m$ -LaH ₁₀ | 200 | 4.36 | 655.6 | 5.0 | 130-135 | 214-234 | 264-276 | 252-271 |
| | 300 | 1.94 | 1380.7 | 5.4 | 181-195 | 211-231 | 250-264 | 210-232 |
| $Fm\bar{3}m$ -YH ₁₀ | 300 | 2.02 | 1444.0 | 4.6 | 196-209 | 231-253 | 277-292 | 235-259 |
| $Im\bar{3}m$ -H ₃ S | 200 | 1.88 | 1266.0 | 3.1 | 162-175 | 186-204 | 212-223 | 206-229 |

^a T_c was estimated using Allen-Dynes modified McMillian equation with $f_1 f_2 = 1$ (Eq. S11).

^b T_c was estimated using Allen-Dynes modified McMillian equation with $f_1 f_2 \neq 1$ (Eq. S12).

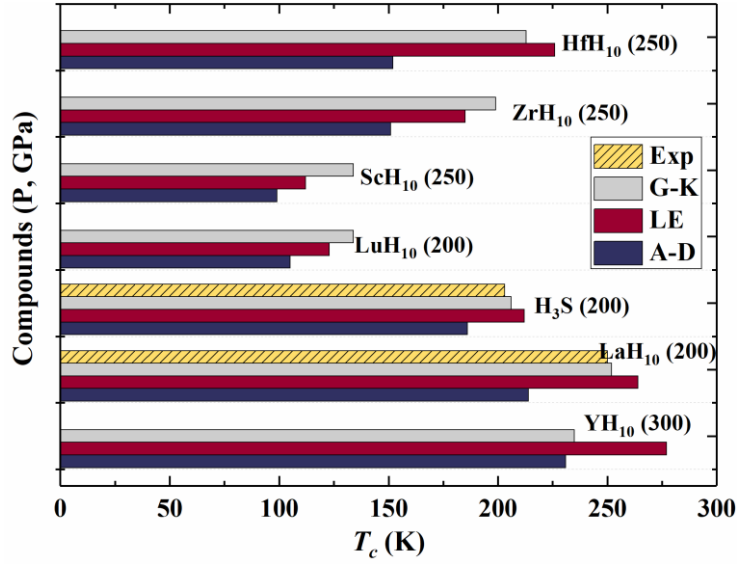


Fig. S7. Comparison of T_c ($\mu^*=0.13$) values obtained by different equations for different hydrogen-rich materials.

Table S5. Calculated isotope effect and superconductive gap of MH₁₀ (M=Hf, Zr, Sc, Lu).

| Parameter | HfH ₁₀ | ZrH ₁₀ | ScH ₁₀ | LuH ₁₀ |
|-------------------|-------------------|-------------------|-------------------|-------------------|
| | 250 GPa | 250 GPa | 250 GPa | 200 GPa |
| α | 0.42-0.43 | 0.38-0.39 | 0.37-0.38 | 0.44-0.45 |
| T_c^D , K | 159-174 | 153-168 | 104-121 | 99-111 |
| $\Delta(0)$, meV | 39.9-45.2 | 35.3-40.0 | 22.1-26.6 | 22.4-25.8 |

Projected DOS and superconductive parameters of the other hafnium hydrides

For HfH_x compounds with $x = 1$ to 4, the hydrogen contribution to the DOS is relatively low at the Fermi level, which results in moderate electron-phonon coupling (EPC). For HfH₆ and $P\bar{1}$ -HfH₁₀, the total DOS at the Fermi level is low, due to orbital splitting during the formation of diatomic/triatomic hydrogen units in the structure. The estimated T_c 's for HfH₁₋₃, as expected, are fairly low with values of < 20 K due to the weak electron-phonon interaction and low logarithmic average frequency (ω_{log}). As the hydrogen content increases, the EPC is strengthened and ω_{log} enhanced. Electron-phonon coupling calculations for HfH₄, HfH₆ and $P\bar{1}$ -HfH₁₀ yield λ of 0.88 (200 GPa), 0.84 (300 GPa) and 0.72 (200 GPa), respectively. The calculated T_c 's are increased to 41.6-50.1, 45.2-55.0 and 28.9-37.4

K using a typical Coulomb potential of $\mu^* = 0.1-0.13$. Although HfH_{10} has the highest hydrogen content, the existence of H_2 units in the $P\bar{1}$ structure reduces the electronic density of states at the Fermi energy, thereby limiting its superconductivity

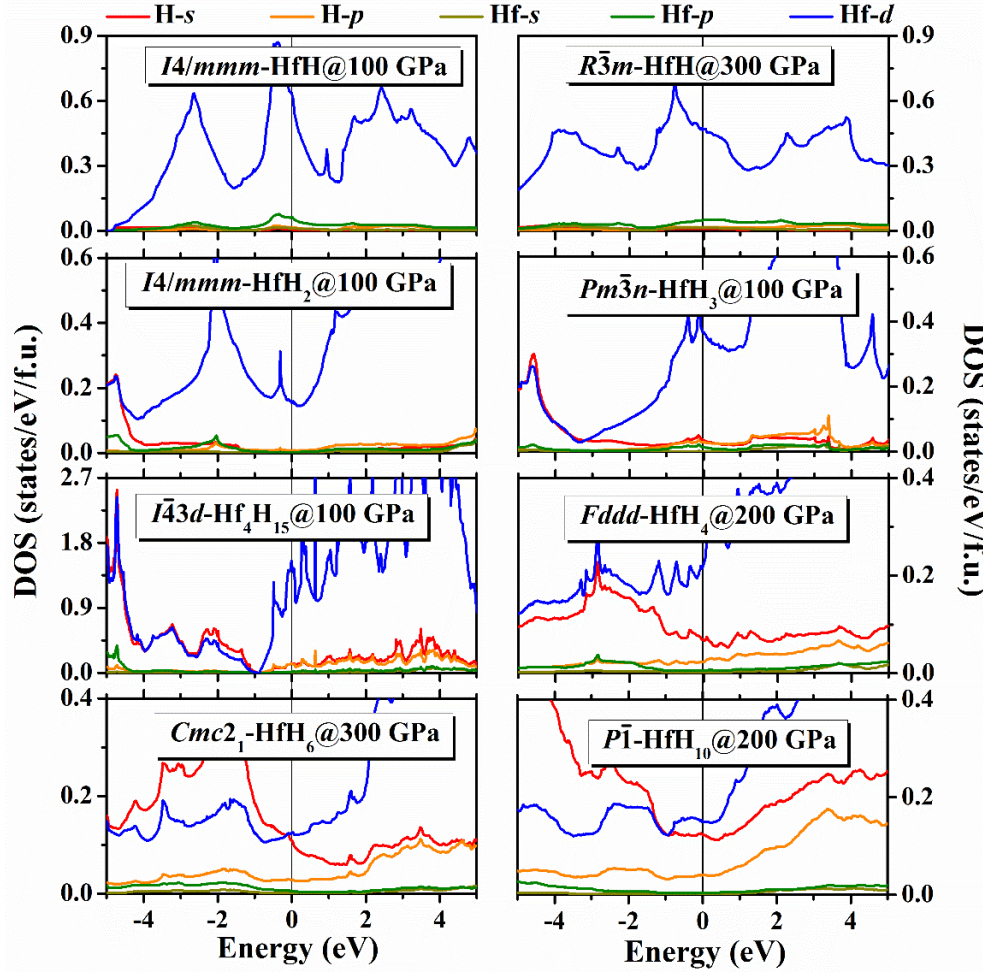


Fig. S8. Calculated projected density of states (DOS) for hafnium hydrides under pressures. All compounds were found to be metallic with the absence of a band gap.

Table S6. The calculated EPC parameter λ , logarithmic average phonon frequency ω_{log} , electronic density of states at Fermi level $N(\epsilon_f)$ (states/spin/Ry/f.u.) and superconducting transition temperatures T_c (K) with $\mu^*=0.1-0.13$ at corresponding pressures P (GPa).

| Structure | P | λ | ω_{log} (K) | $N(\epsilon_f)$ | T_c (K) |
|---------------------------------------|-----|-----------|--------------------|-----------------|-----------|
| $I4/mmm\text{-HfH}$ | 100 | 0.68 | 270.8 | 6.5 | 6.8-8.9 |
| $R\bar{3}m\text{-HfH}$ | 300 | 1.24 | 157.6 | 5.2 | 13.0-14.6 |
| $I4/mmm\text{-HfH}_2$ | 100 | 0.15 | 382.8 | 2.1 | 0 |
| $Pm\bar{3}n\text{-HfH}_3$ | 100 | 0.62 | 582.6 | 4.3 | 10.6-14.7 |
| $I\bar{4}3d\text{-Hf}_4\text{H}_{15}$ | 100 | 0.37 | 791.1 | 12.1 | 0.8-2.1 |

| | | | | | |
|----------------------------|-----|------|--------|-----|-----------|
| $Fddd\text{-HfH}_4$ | 200 | 0.88 | 892.3 | 3.3 | 41.4-50.1 |
| $Cmc2_1\text{-HfH}_6$ | 300 | 0.84 | 1057.2 | 2.5 | 45.2-55.0 |
| $P\bar{1}\text{-HfH}_{10}$ | 200 | 0.72 | 1013.9 | 3.3 | 28.9-37.4 |
| | 300 | 0.66 | 1207.4 | 2.9 | 26.8-36.1 |

MgH₁₀ and ThH₁₀

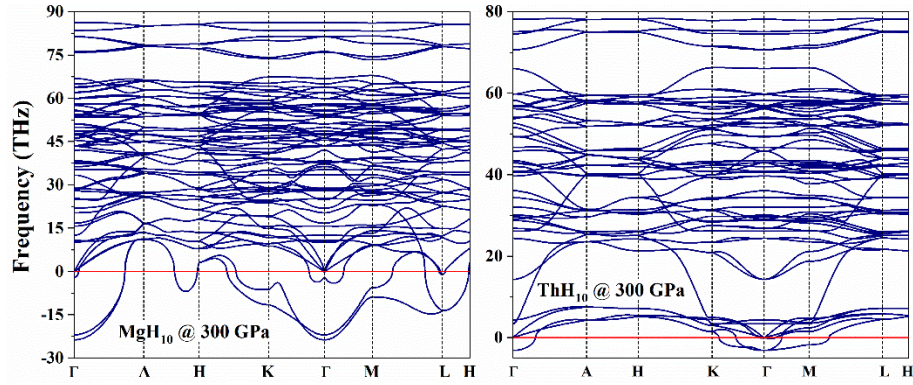


Fig. S9. Phonon spectrum of $P6_3/mmc\text{-MgH}_{10}$ and $P6_3/mmc\text{-ThH}_{10}$ at 300 GPa. There are imaginary phonon frequencies for the two structures, indicating their dynamic instabilities

ScH₁₀

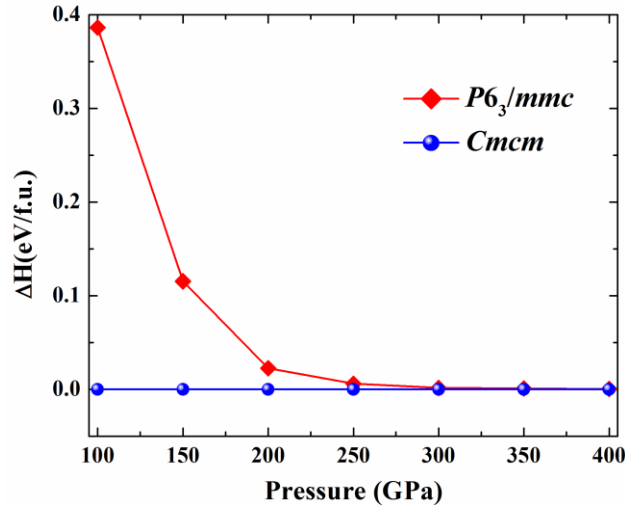


Fig. S10. Calculated enthalpy of $P6_3/mmc$ structure relative to $Cmcm$ in ScH_{10} .

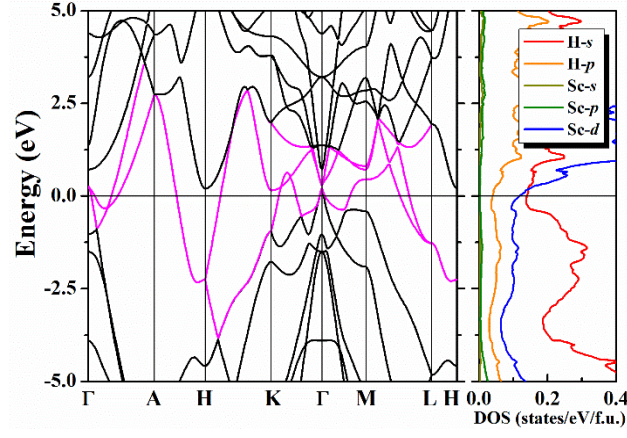


Fig. S11. Calculated electronic band structures and projected DOS of $P6_3/mmc$ -ScH₁₀ at 250 GPa.

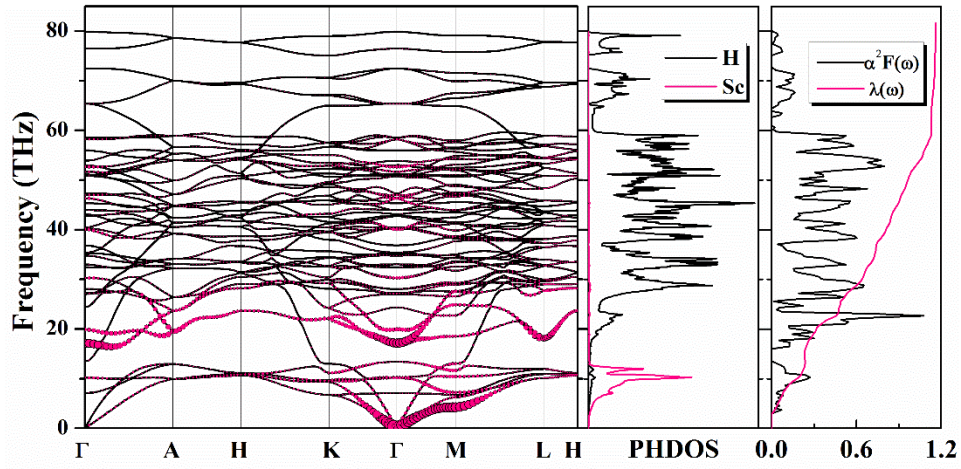


Fig. S12. Phonon dispersion curves, phonon density of states and Eliashberg spectral function $\alpha^2 F(\omega)$ together with the electron-phonon integral $\lambda(\omega)$ of $P6_3/mmc$ -ScH₁₀ at 250 GPa. The absence of imaginary frequency confirms its dynamic stability.

LuH₁₀

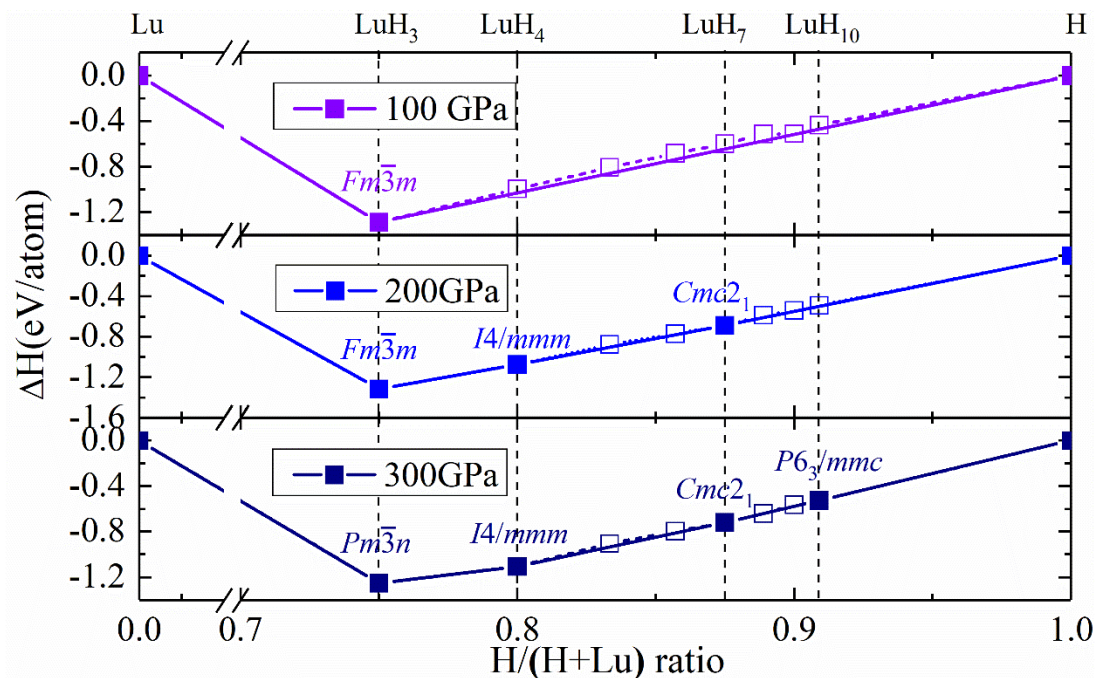


Fig. S13. Predicted formation enthalpies of LuH_n (n=3-10) not inclusion ZPE with respect to decomposition into Lu and H₂ under pressure. LuH₃ is predicted to be stable with $Fm\bar{3}m$ symmetry from 100 GPa to 200 GPa, then transforms into $Pm\bar{3}n$ at 300 GPa. LuH₄ is stabilized in a $I4/mmm$ structure at 200 GPa, and remains such so up to at least 300 GPa. LuH₇ adopts the $Cmc2_1$ structure in the pressure range of 200-300 GPa. $P6_3/mmc$ -LuH₁₀ is only stable at 300 GPa.

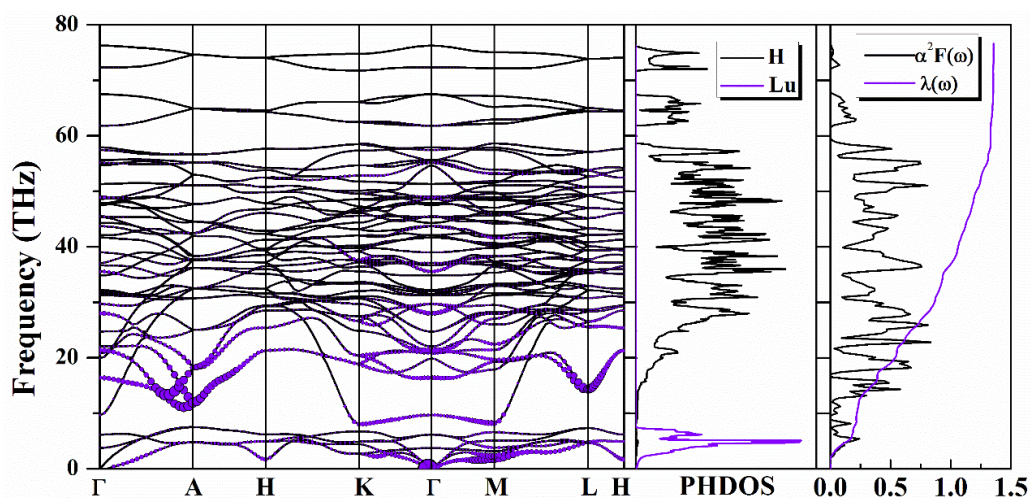


Fig. S14. Phonon dispersion curves, phonon density of states and Eliashberg spectral function $\alpha^2F(\omega)$ together with the electron-phonon integral $\lambda(\omega)$ of $P6_3/mmc$ -LuH₁₀ at 200 GPa. The absence of imaginary frequency confirms its dynamic stability.

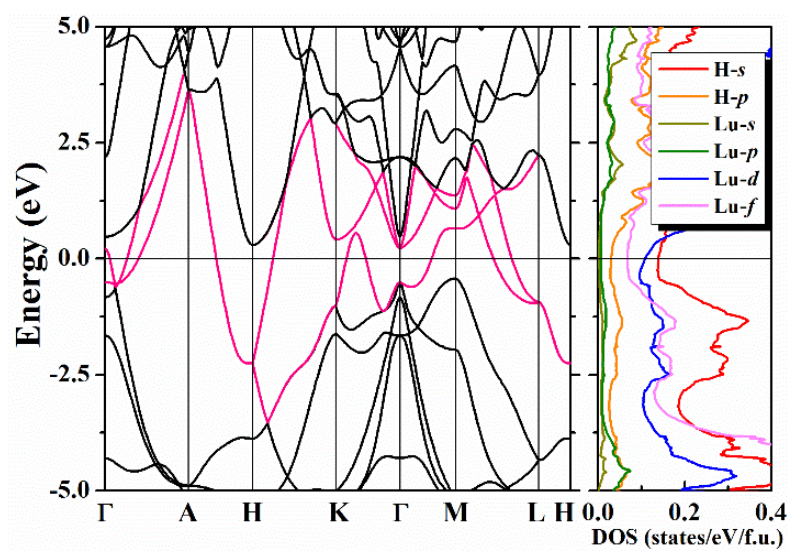


Fig. S15. Calculated electronic band structures and projected DOS of $P6_3/mmc$ -LuH₁₀ at 200 GPa.

Dynamic stability

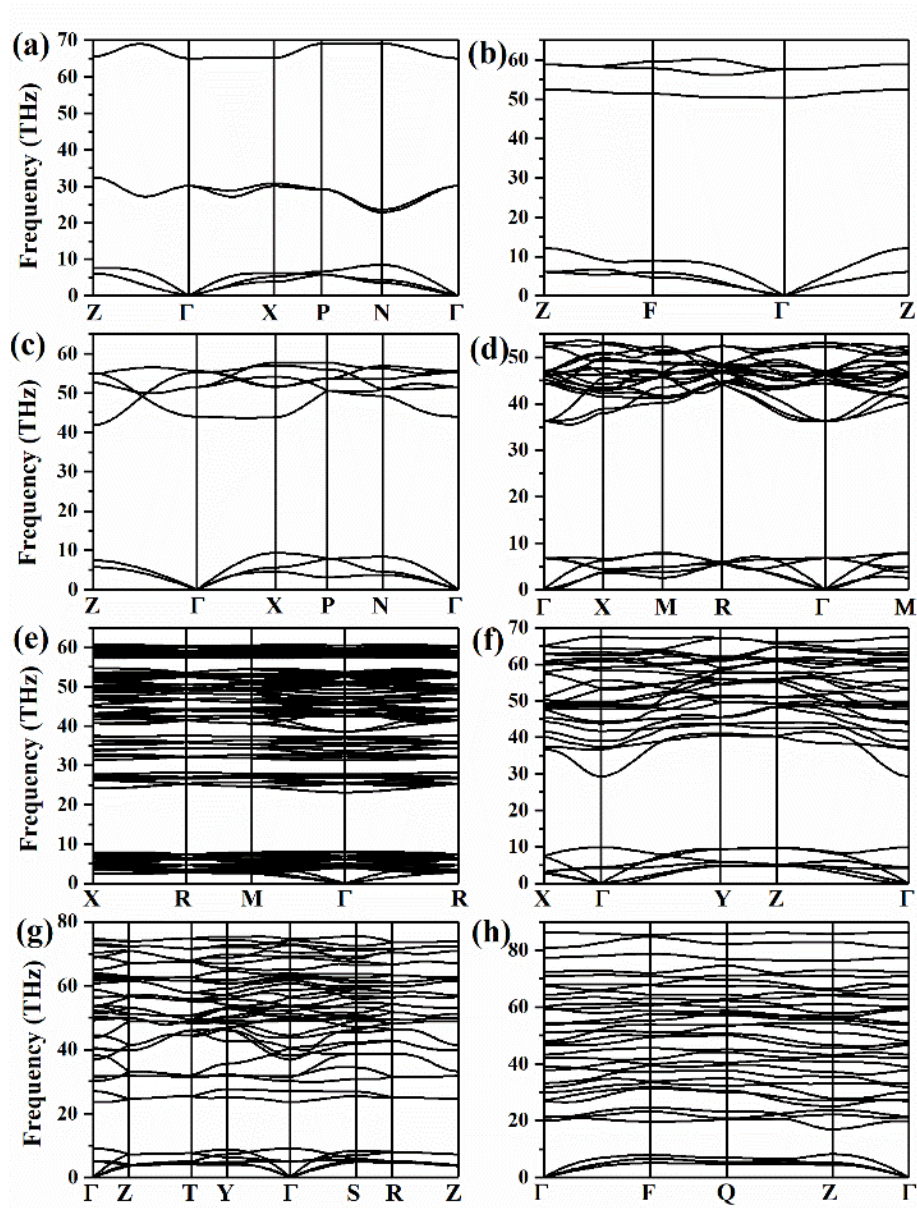


Fig. S16. The calculated phonon dispersion curves of (a) $I4/mmm$ -HfH at 100 GPa, (b) $R\bar{3}m$ -HfH, (c) $I4/mmm$ -HfH₂ at 100 GPa, (d) $Pm\bar{3}n$ -HfH₃ at 100 GPa, (e) $I\bar{4}3d$ -Hf₄H₁₅ at 100 GPa, (f) $Fddd$ -HfH₄ at 300 GPa, (g) $Cmc2_1$ -HfH₆ at 300 GPa, (h) $P\bar{1}$ -HfH₁₀ at 300 GPa. The absence of imaginary frequency of Hf hydrides confirms their dynamic stabilities.

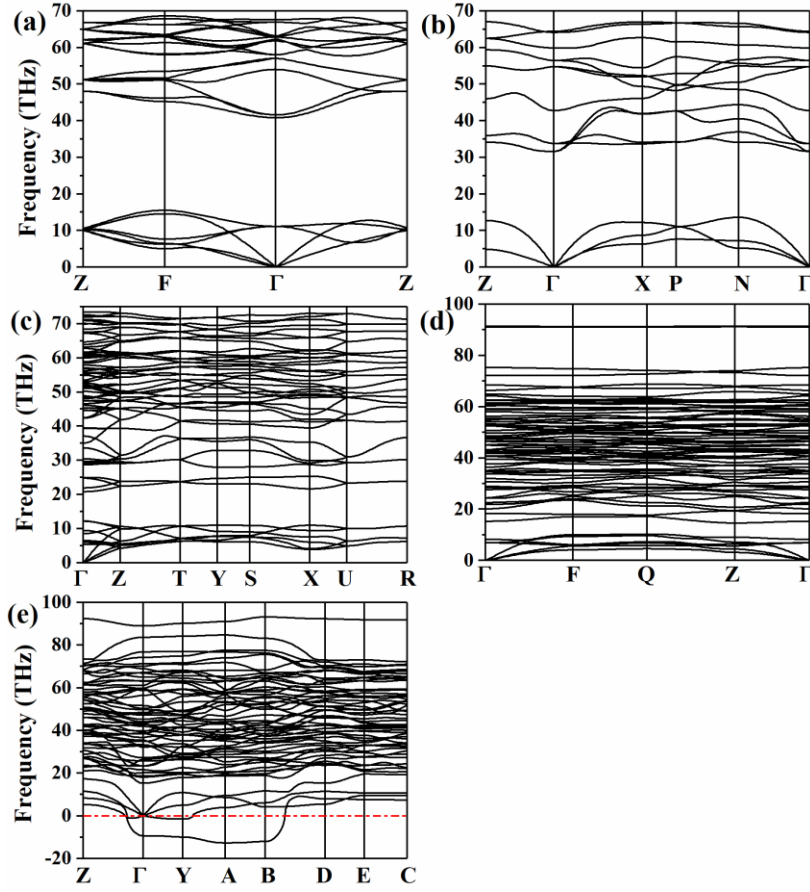


Fig. S17. The calculated phonon dispersion curves of (a) $R\bar{3}c$ -ZrH₃, (b) $I4/mmm$ -ZrH₄, (c) $Cmc2_1$ -ZrH₆, (d) $P\bar{1}$ -ZrH₁₀ and (e) $P2/m$ -ZrH₁₇ at 300 GPa. The absence of imaginary frequency in ZrH₃, ZrH₄, ZrH₆ and ZrH₁₀ suggests their dynamic stabilities, while ZrH₁₇ is unstable due to the appearance of negative phonon mode.

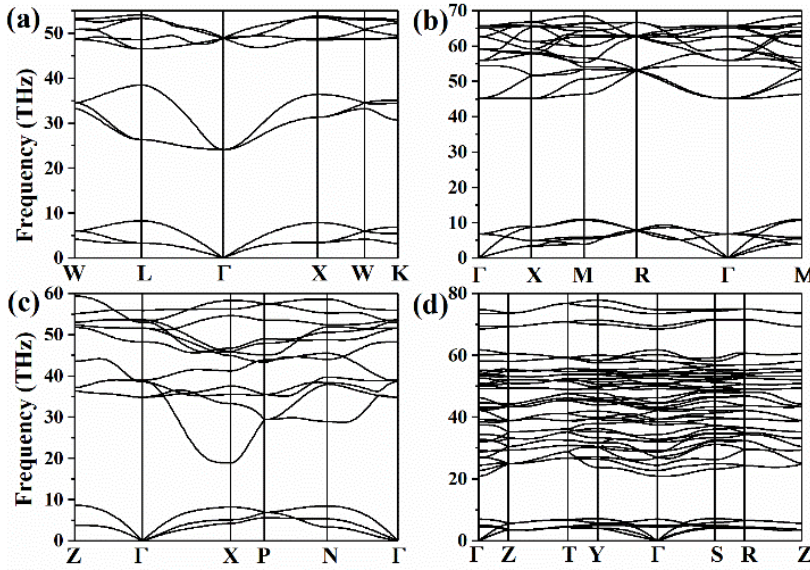


Fig. S18. The calculated phonon dispersion curves of (a) $Fm\bar{3}m$ -LuH₃ at 100 GPa, (b) $Pm\bar{3}n$ -LuH₃ at 300 GPa, (c) $I4/mmm$ -LuH₄ at 200 GPa and (d) $Cmc2_1$ -LuH₇ at 200 GPa. The absence of imaginary frequency of Lu hydrides confirms their dynamic stabilities.

EOS for $M\text{H}_3$ (M=Hf, Zr and Lu)

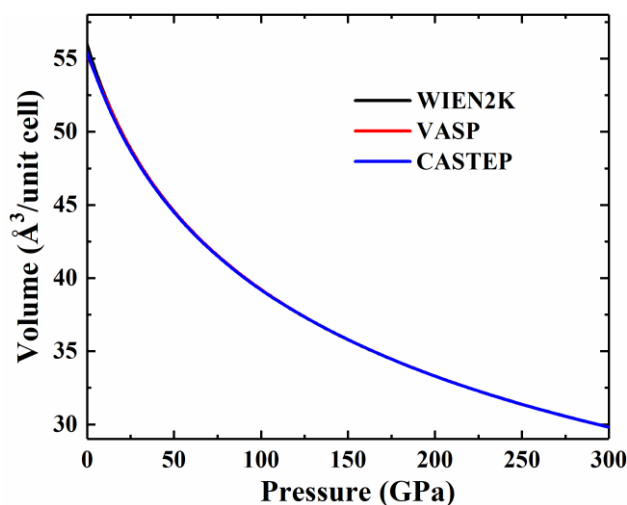


Fig. S20. Volumes as a function of pressures for $Pm\bar{3}n\text{-HfH}_3$ calculated by using PAW potential in VASP calculations, OTF potentials in CASTEP calculations and full-potential in WIEN2K calculations. The GGA_PBE exchange correlation functional was chosen in the three calculations, giving identical results. The purpose of this comparison is to test the validity of pseudopotentials in geometrical optimization and ZPE calculations below 300 GPa.

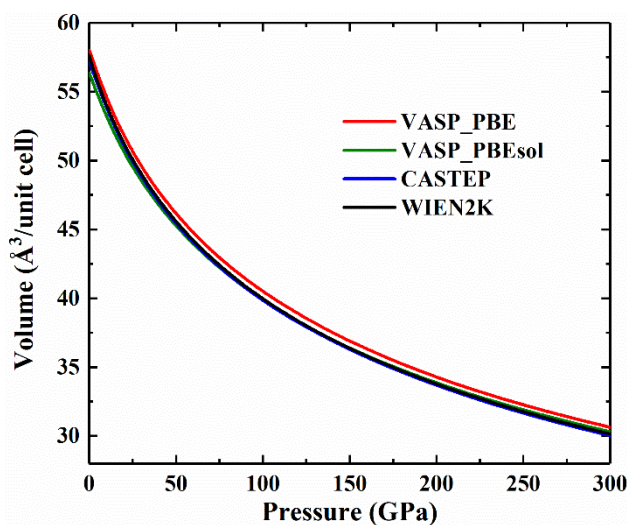


Fig. S21. Volumes as a function of pressures for $Pm\bar{3}n\text{-ZrH}_3$ calculated by using PAW potential (GGA_PBE and GGA_PBEsol exchange correlation functional) in VASP calculations, OTF potentials in CASTEP calculations and full-potential in WIEN2K. It is found that OTF potentials, PAW (GGA_PBEsol) potentials and full-potential calculations gave identical results, but VASP calculations with GGA_PBE exchange correlation functional deviate.

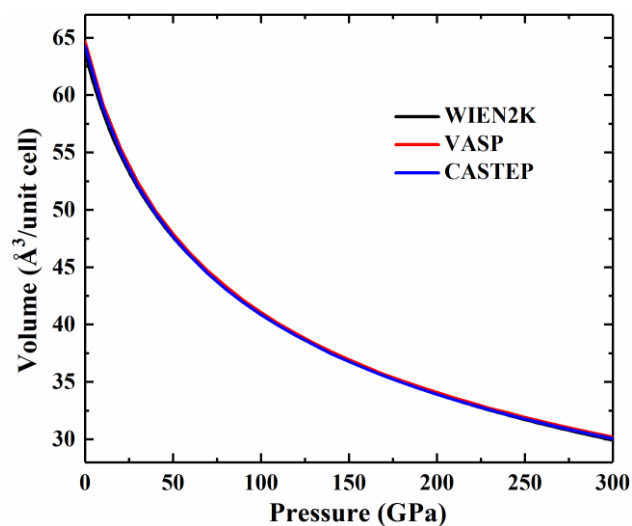


Fig. S22. Volumes as a function of pressures for $Pm\bar{3}n$ -LuH₃ calculated by using PAW potential in VASP calculations, OTF potentials in CASTEP calculations and full-potential in WIEN2K calculations. The GGA_PBE exchange correlation functional was chosen in the three calculations, giving identical results. The purpose of this calculation is to test the validity of the PAW potentials adopted under pressures up to 300 GPa.

Structural information

Table S7. Structural information of predicted hydrides.

| Space group Pressure | Lattice parameters (Å, °) | Atomic coordinates (fractional) | | | | Sites |
|--|---|---------------------------------|--------|--------|--------|-------|
| <i>I4/mmm</i> -HfH 100 GPa | a = 2.911 | H1 | 0.000 | 0.000 | 0.000 | 2a |
| | b = 2.911 | Hf1 | 0.000 | 0.000 | 0.500 | 2b |
| | c = 3.676 | | | | | |
| | $\alpha = \beta = \gamma = 90$ | | | | | |
| <i>R$\bar{3}m$</i> -HfH 300 GPa | a = 2.694 | H1 | 0.000 | 0.000 | 1.000 | 3a |
| | b = 2.694 | Hf1 | 0.000 | 0.000 | 0.500 | 3b |
| | c = 5.677 | | | | | |
| | $\alpha = \beta = 90$ $\gamma = 120$ | | | | | |
| <i>I4/mmm</i> -HfH ₂ 100 GPa | a = 3.222 | H1 | 0.500 | 0.000 | 0.250 | 4d |
| | b = 3.222 | Hf1 | 0.000 | 0.000 | 0.000 | 2a |
| | c = 3.433 | | | | | |
| | $\alpha = \beta = \gamma = 90$ | | | | | |
| <i>Pm$\bar{3}n$</i> -HfH ₃ 100 GPa | a = 3.368 | H1 | -0.500 | 1.250 | -2.000 | 6c |
| | b = 3.368 | Hf1 | 0.000 | 0.000 | -1.000 | 2a |
| | c = 3.368 | | | | | |
| | $\alpha = \beta = \gamma = 90$ | | | | | |
| <i>I$\bar{4}3d$</i> -Hf ₄ H ₁₅ 100 GPa | a = 7.017 | H1 | 0.284 | 0.073 | 0.149 | 48e |
| | b = 7.017 | H25 | -0.125 | -0.000 | 0.250 | 12b |
| | c = 7.017 | Hf1 | 0.043 | 0.043 | 0.043 | 16c |
| | $\alpha = \beta = \gamma = 90$ | | | | | |
| <i>Fddd</i> -HfH ₄ 200 GPa | a = 10.180 | H1 | 0.171 | 0.085 | 1.764 | 32h |
| | b = 4.839 | Hf1 | -0.250 | 0.750 | 1.250 | 8a |
| | c = 2.912 | | | | | |
| | $\alpha = \beta = \gamma = 90$ | | | | | |
| <i>Cmc2₁</i> -HfH ₆ 300 GPa | a = 2.917 | H1 | -0.217 | -0.575 | -0.018 | 8b |
| | b = 5.482 | H5 | 0.000 | -0.641 | -0.311 | 4a |
| | c = 4.818 | H6 | 0.000 | -0.845 | 0.004 | 4a |
| | $\alpha = \beta = \gamma = 90$ | H7 | 0.000 | -0.896 | -0.410 | 4a |
| | | H11 | 0.000 | -0.008 | -0.221 | 4a |
| | | Hf1 | 0.000 | -0.322 | -0.203 | 4a |
| <i>P$\bar{1}$</i> -HfH ₁₀ 300 GPa | a = 2.731 | H1 | 0.455 | 0.022 | -0.187 | 2i |
| | b = 2.831 | H2 | -0.307 | 0.467 | -0.058 | 2i |
| | c = 3.626 | H3 | -0.225 | 1.053 | -0.952 | 2i |
| | $\alpha = 103.41$ | H4 | 0.126 | 0.405 | -0.838 | 2i |
| | $\beta = 87.13$ | H5 | -0.321 | 0.568 | -0.642 | 2i |
| | $\gamma = 66.40$ | Hf6 | -0.000 | 0.000 | -0.500 | 1b |

| | | | | | | |
|---|-----------------------|-----|-------|-------|--------|-----|
| <i>P6₃/mmc</i> -HfH ₁₀ 300 GPa | a = 4.633 | H1 | 0.375 | 0.077 | 0.250 | 12j |
| | b = 4.633 | H13 | 0.885 | 0.115 | 0.750 | 6h |
| | c = 2.607 | H19 | 0.000 | 0.000 | 0.250 | 2b |
| | $\alpha = \beta = 90$ | Hf1 | 0.667 | 0.333 | 0.750 | 2c |
| | $\gamma = 120$ | | | | | |
| <i>P6₃/mmc</i> -ZrH ₁₀ 300 GPa | a = 4.661 | H1 | 0.370 | 0.076 | 0.250 | 12j |
| | b = 4.661 | H13 | 0.886 | 0.114 | 0.7500 | 6h |
| | c = 2.631 | H19 | 0.000 | 0.000 | 0.250 | 2b |
| | $\alpha = \beta = 90$ | Zr1 | 0.667 | 0.333 | 0.750 | 2c |
| | $\gamma = 120$ | | | | | |
| <i>P6₃/mmc</i> -ScH ₁₀ 250 GPa | a = 4.559 | H1 | 0.384 | 0.080 | 0.250 | 12j |
| | b = 4.559 | H13 | 0.882 | 0.118 | 0.750 | 6h |
| | c = 2.635 | H19 | 0.000 | 0.000 | 0.250 | 2b |
| | $\alpha = \beta = 90$ | Sc1 | 0.667 | 0.333 | 0.750 | 2c |
| | $\gamma = 120$ | | | | | |
| <i>P6₃/mmc</i> -LuH ₁₀ 200 GPa | a = 4.806 | H1 | 0.626 | 0.705 | 0.7500 | 12j |
| | b = 4.806 | H13 | 0.886 | 0.771 | 0.750 | 6h |
| | c = 2.784 | H19 | 0.000 | 0.000 | 0.250 | 2b |
| | $\alpha = \beta = 90$ | Lu1 | 0.667 | 0.333 | 0.750 | 2c |
| | $\gamma = 120$ | | | | | |

References

1. Pickard, C. J. & Needs, R. J. Ab initio random structure searching. *J. Phys.: Condens. Matter* **23**, 053201 (2011).
2. Wang, Y., Lv, J., Zhu, L. & Ma, Y. Crystal structure prediction via particle-swarm optimization. *Phys. Rev. B* **82**, 094116 (2010).
3. Wang, Y., Lv, J., Zhu, L. & Ma, Y. CALYPSO: A method for crystal structure prediction. *Comput. Phys. Commun.* **183**, 2063-2070 (2012).
4. Lyakhov, A. O., Oganov, A. R., Stokes, H. T. & Zhu, Q. New developments in evolutionary structure prediction algorithm USPEX. *Comput. Phys. Commun.* **184**, 1172-1182 (2013).
5. Oganov, A. R. & Glass, C. W. Crystal structure prediction using ab initio evolutionary techniques: Principles and applications. *J. Chem. Phys.* **124**, 244704 (2006).
6. Oganov, A. R., Lyakhov, A. O. & Valle, M. How Evolutionary Crystal Structure Prediction Works—and Why. *Acc. Chem. Res.* **44**, 227-237 (2011).
7. Segall, M. D. et al. First-principles simulation: ideas, illustrations and the CASTEP code. *J. Phys.: Condens. Matter* **14**, 2717 (2002).
8. Kresse, G. & Joubert, D. From ultrasoft pseudopotentials to the projector augmented-wave method. *Phys. Rev. B* **59**, 1758-1775 (1999).
9. Kresse, G. & Furthmüller, J. Efficiency of ab-initio total energy calculations for metals and semiconductors using a plane-wave basis set. *Comput. Mater. Sci.* **6**, 15-50 (1996).
10. Perdew, J. P., Burke, K. & Ernzerhof, M. Generalized Gradient Approximation Made Simple. *Phys. Rev. Lett.* **77**, 3865-3868 (1996).
11. Perdew, J. P. & Wang, Y. Accurate and simple analytic representation of the electron-gas correlation energy. *Phys. Rev. B* **45**, 13244-13249 (1992).
12. Monkhorst, H. J. & Pack, J. D. Special points for Brillouin-zone integrations. *Phys. Rev. B* **13**, 5188-5192 (1976).
13. Blaha, P., Schwarz, K., Sorantin, P. & Trickey, S. Full-potential, linearized augmented plane wave programs for crystalline systems. *Comput. Phys. Commun.* **59**, 399-415 (1990).
14. Birch, F. The Effect of Pressure Upon the Elastic Parameters of Isotropic Solids, According to Murnaghan's Theory of Finite Strain. *J. Appl. Phys.* **9**, 279-288 (1938).
15. Becke, A. D. & Edgecombe, K. E. A simple measure of electron localization in atomic and molecular systems. *J. Chem. Phys.* **92**, 5397-5403 (1990).
16. Dronskowski, R. & Bloechl, P. E. Crystal orbital Hamilton populations (COHP): energy-resolved visualization of chemical bonding in solids based on density-functional calculations. *J. Phys. Chem.* **97**, 8617-8624 (1993).
17. Henkelman, G., Arnaldsson, A. & Jónsson, H. A fast and robust algorithm for Bader decomposition of charge density. *Computational Materials Science* **36**, 354-360 (2006).
18. Tang, W., Sanville, E. & Henkelman, G. A grid-based Bader analysis algorithm without lattice bias. *J. Phys.: Condens. Matter* **21**, 084204 (2009).
19. Togo, A., Oba, F. & Tanaka, I. First-principles calculations of the ferroelastic transition between rutile-type and CaCl_2 -type SiO_2 at high pressures. *Phys. Rev. B* **78**, 134106 (2008).
20. Perdew, J. P. et al. Restoring the Density-Gradient Expansion for Exchange in Solids and Surfaces. *Phys. Rev. Lett.* **100**, 136406 (2008).
21. Paolo, G. et al. QUANTUM ESPRESSO: a modular and open-source software project for quantum simulations of materials. *J. Phys.: Condens. Matter* **21**, 395502 (2009).

22. Troullier, N. & Martins, J. L. Efficient pseudopotentials for plane-wave calculations. *Phys. Rev. B* **43**, 1993-2006 (1991).
23. Eliashberg, G. Interactions between electrons and lattice vibrations in a superconductor. *Sov. Phys. JETP* **11**, 696-702 (1960).
24. Allen, P. B. & Dynes, R. C. Transition temperature of strong-coupled superconductors reanalyzed. *Phys. Rev. B* **12**, 905-922 (1975).
25. Gor'kov, L. P. & Kresin, V. Z. Pressure and high- T_c superconductivity in sulfur hydrides. *Sci. Rep.* **6**, 25608 (2016).
26. Gor'kov, L. P. & Kresin, V. Z. Colloquium: High pressure and road to room temperature superconductivity. *Rev. Mod. Phys.* **90**, 011001 (2018).
27. Bergmann, G. & Rainer, D. The sensitivity of the transition temperature to changes in $\alpha^2 F(\omega)$. *Z. Phys.* **263**, 59-68 (1973).
28. Rainer, D. & Bergmann, G. Temperature dependence of H_{c2} and κ_1 in strong coupling superconductors. *J. Low Temp. Phys.* **14**, 501-519 (1974).
29. Allen, P. B. A computer program for numerical solution of the Eliashberg equation to find T_c , Tech. Rep. 7 TCM41974 (1974).
30. Kruglov, I. A. et al. Superconductivity of LaH₁₀ and LaH₁₆ polyhydrides. *Phys. Rev. B* **101**, 024508 (2020).
31. Allen, P. B. Neutron Spectroscopy of Superconductors. *Phys. Rev. B* **6**, 2577-2579 (1972).
32. Duan, D. et al. Pressure-induced metallization of dense (H₂S)₂H₂ with high- T_c superconductivity. *Sci. Rep.* **4**, 6968 (2014).
33. Drozdov, A. P., Erements, M. I., Troyan, I. A., Ksenofontov, V. & Shylin, S. I. Conventional superconductivity at 203 kelvin at high pressures in the sulfur hydride system. *Nature* **525**, 73-76 (2015).
34. Zhang, S. et al. Phase Diagram and High-Temperature Superconductivity of Compressed Selenium Hydrides. *Sci. Rep.* **5**, 15433 (2015).
35. Peng, F. et al. Hydrogen Clathrate Structures in Rare Earth Hydrides at High Pressures: Possible Route to Room-Temperature Superconductivity. *Phys. Rev. Lett.* **119**, 107001 (2017).
36. Drozdov, A. P. et al. Superconductivity at 250 K in lanthanum hydride under high pressures. *Nature* **569**, 528-531 (2019).
37. Somayazulu, M. et al. Evidence for Superconductivity above 260 K in Lanthanum Superhydride at Megabar Pressures. *Phys. Rev. Lett.* **122**, 027001 (2019).
38. Kvashnin, A. G., Semenov, D. V., Kruglov, I. A., Wrona, I. A. & Oganov, A. R. High-Temperature Superconductivity in a Th-H System under Pressure Conditions. *ACS Appl. Mater. Interfaces* **10**, 43809-43816 (2018).
39. Semenov, D. V. et al. Superconductivity at 161 K in thorium hydride ThH₁₀: Synthesis and properties. *Mater. Today*, <https://doi.org/10.1016/j.mattod.2019.10.005> (2019).